Journal of Neuroscience Methods 130 (2003) 173–199

JOURNAL OF NEUROSCIENCE METHODS

www.elsevier.com/locate/jneumeth

Combining principal component and spectral analyses with the method of moments in studies of quantal transmission

Alexander E. Dityatev [a,*], Radik Sh. Altinbaev [b], Andrej V. Astrelin [c], Leon L. Voronin [b]

[a] *Zentrum für Molekulare Neurobiologie, Universität Hamburg, Martinistr. 52, D-20246 Hamburg, Germany*
[b] *Brain Research Institute, Academy of Medical Sciences and Institute of Higher Nervous Activity and Neurophysiology, Russian Academy of Sciences, Butlerova 5a, 117485 Moscow, Russia*
[c] *Department of Mathematics and Mechanics, Moscow State University, Vorobiovy Gory, 119899 Moscow, Russia*

Accepted 8 September 2003

Abstract

This chapter considers methods for measurements of postsynaptic responses and simple approaches to the estimation of parameters of quantal release in synapses of the central nervous system of vertebrates. The use of these methods is illustrated by the analysis of single-fibre and "minimal" monosynaptic postsynaptic potentials (PSPs) or currents (PSCs) recorded from neurons of the frog spinal cord and rat hippocampus. First, we briefly discuss traditional methods of the response measurements using peak amplitudes or areas, further focusing on a novel method based on multivariate statistical techniques of the principal component analysis (PCA). This approach provides typically better signal-to-noise ratios and is able to separate two or more response components, which can arise due to activation of more than one presynaptic fibre, axon collaterals, receptor subtypes or spatially separated transmission sites. Second, spectral analysis is introduced as the method of choice to verify whether the amplitude fluctuations of the postsynaptic responses have a quantal nature and to obtain estimations of the "basic" quantal parameters, i.e. the quantal size (Q) and mean quantal content (m), without introducing assumptions on release statistics. Third, we show how the method of moments could be applied in the framework of the Poisson and binomial models to estimate the basic quantal parameters and parameters p and n, which reflect the release probability and maximum number of quanta released (or the number of effective release sites), respectively. Fourth, we show that the analysis of the moments can also be instrumental to reveal non-uniformity of release probabilities and compare how several competing models of neurotransmitter release fit to multiple experimental data sets.

Keywords: Synaptic transmission; Postsynaptic response; Principal component analysis; Spectral analysis; Quantal analysis; Method of moments; Long-term potentiation; Hippocampus; Spinal cord

1. Introduction

Quantal theory of synaptic transmission (del Castillo and Katz, 1954a, 1954b) has been based on the observation that when the mean probability of transmitter release (p) is low, the amplitudes of a postsynaptic response vary randomly between integer multiplies of spontaneous "miniature" responses (called also "minis"). Basics of the quantal theory are described in several excellent reviews (Auger and Marty, 2000; Bekkers and Stevens, 1991; Jack et al., 1994; Korn and Faber, 1987, 1991; Redman, 1990; Stevens, 1993; Thomson, 2000; Thomson and Deuchars, 1995; Walmsley, 1993) and handbooks (e.g. Nicholls et al., 2001; see also Voronin, 1993a, 1993b and especially other chapters for more recent data and additional discussion).

Quantal analysis includes a number of statistical methods aimed to evaluate both the basic quantal parameters (Q and m), and number of release sites or vesicles immediately available for release (n) and mean release probability (p) of a synapse under study. Data sets for the statistical treatments are provided by electrophysiological recordings of postsynaptic responses. The aim of the initial Sections 1 and 2 of this chapter is to briefly consider related recording and measurement methods. Several common methods of measurements are briefly considered followed by the detailed presentation of the amplitude measurements based on the principal component analysis (PCA) that has also been modified by the authors to extract response components likely

* Corresponding author. Tel.: +49-40-428036250; fax: +49-40-428036302.
E-mail address: dityatev@zmnh.uni-hamburg.de (A.E. Dityatev).

0165-0270/$ – see front matter © 2003 Elsevier B.V. All rights reserved.
doi:10.1016/j.jneumeth.2003.09.022

Nomenclature

AMPA	α-amino-3-hydroxy-5-methyl-4-isoxazole propionic acid
APV	D-2-amino-5-phosphonovalerate
C1, C2, C3	components 1, 2 and 3, respectively
C2/C1 plot	plot of the scores of C2 against C1
CNQX	6-cyano-7-nitroquinoxaline-2,3-dione
CNS	central nervous system
CV	coefficient of variation
E_i	ith amplitude measurement
E_{max}	maximum amplitude
EPSC	excitatory postsynaptic current
EPSP	excitatory postsynaptic potential
F_j	theoretical frequency
H_j	empirical frequency
L	latency
LTP	long-term potentiation
m	mean quantal content
M_1, M_2, M_3	central moments of a distribution
n	binomial parameter n, maximum number of vesicles that can be released, number of functional release sites
N	sample size, number of measurements in a data set
N_0	number of transmission failures
NMDA	*N*-methyl-D-aspartate
p	binomial parameter p, probability of release
p_k	probability of release at kth release site
P	level of significance
PCA	principal component analysis
PDF	probability density function
PSC	postsynaptic current
PSP	postsynaptic potential
Q	quantal size
r	coefficient of correlation
R_1, R_2	ratios between moments
S_{max}	maximum of spectral density
S_n	standard deviation of noise
T_{decay}	decay time
T_{rise}	rise time
χ^2	chi-square statistics

mediated by different synapses or subtypes of glutamate receptors. Section 3 describes the use of spectral analysis for evaluation of the response fluctuations and basic quantal parameters. The final part of this chapter introduces the analysis of moments of amplitude distributions aimed to select an appropriate model and to evaluate parameters of quantal release. More detailed description of the commonly used methods and additional references can be found in above cited reviews and in other chapters of this issue (for related publications from our groups, see Astrelin et al., 1997, 1998; Berretta et al., 1999, 2000; Dityatev and Clamann, 1998; Dityatev et al., 1994, 2001a, 2001b; Kasyanov et al., 2000; Sokolov et al., 2002, 2003; Voronin et al., 1999; also see Voronin, 1993a, 1993b, 1994 for references to earlier publications).

2. Recordings and traditional measurements of postsynaptic responses

2.1. Recordings of unitary and minimal postsynaptic responses

A postsynaptic response induced by activation of a single presynaptic neuron or axon is called “single-fibre” or “unitary” (or “elementary”) response. Recordings of unitary responses provide the most suitable data for quantal analysis. Despite difficulties inherent to CNS synapses, a number of laboratories have successfully recorded unitary responses from hippocampal and neocortical slice preparations (Feldmeyer and Sakmann, 2000; Foster and McNaughton, 1991; Malinow, 1991; Markram et al., 1997; Sayer et al., 1990; Stricker et al., 1996a, 1996b). However, the percentage of synaptically connected pairs in slices is very low and examples of quantal analyses of unitary hippocampal postsynaptic potentials or currents (EPSPs or EPSCs) are exceptional (e.g. Foster and McNaughton, 1991). The percentage of connected neuronal pairs is much higher in dissociated or organotypic hippocampal culture. Thus about 50% of CA3 pyramidal neurons have been found to be synaptically connected in the cultured hippocampal slices (Debanne et al., 1996). Therefore, this preparation is more practical for recordings of unitary responses (see Saviane et al., 2002 with references). However, it should be kept in mind that properties of cultured synapses could differ from those in the acutely prepared slices. From our personal experience, the synapses in the hippocampal slices are closer in their properties to hippocampal synapses in vivo although this problem is open to discussion. Studies on the living brain are much more difficult, although intracellular recordings of minimal EPSPs from CA3 neurons in vivo have been published, including application of quantal analysis to LTP (Voronin, 1983, 1993a, 1993b).

One more preparation used to record unitary PSCs of central synapses is the isolated spinal cord of several species (reviewed by Redman, 1990). For instance, isolated spinal cord of the frog have been used for quantal analysis of unitary EPSPs (Babalian and Chmykhova, 1987; Dityatev et al., 1992, 1994, 2001a, 2001b; Grantyn et al., 1984) even with triple intracellular recordings (Dityatev and Clamann, 1998). Properties of two synapses on two different motoneurons innervated by the same presynaptic fibre have been compared in the latter publication. An example of a recently elaborated preparation is the calyx of Held of the rat auditory system (Neher and Sakaba, 2001; Schneggenburger et al.,

2002; von Gersdorff and Borst, 2002; see also the chapter of Neher and Sakaba, 2003). In this preparation, not only may a single presynaptic fibre be activated but also intracellular recording from the giant presynaptic ending is possible together with simultaneous recordings of postsynaptic responses. However, such a preparation is rare in the mammalian CNS. Therefore, recordings of so-called "minimal" postsynaptic potentials (PSPs)/postsynaptic currents (PSCs) are often used, whereby a just supra-threshold stimulus current is selected for extracellular stimulation with the aim of activating a single presynaptic fibre. Minimal stimulation remains as a basic approach to collect data for quantal analysis, although in practice activation of more than one fibre cannot be excluded (Raastad, 1995; Torii et al., 1997).

Up to now, in vitro cortical slices represent the most popular preparations for studies of central synapses in mammals and especially of their short- and long-term plasticity like long-term potentiation (LTP). The latter represents a popular experimental paradigm widely used to study long-term synaptic plasticity and information storage in CNS (Bliss and Collingridge, 1993; Malenka and Nicoll, 1999). Fig. 1A and B illustrates two basic types of synaptic connections most commonly analyzed in hippocampal slices. In experiments with recordings from CA1 or CA3 pyramidal neurons, stimulating electrodes are placed to activate Schaffer collaterals or mossy fibres (Fig. 1A and B, respectively). Recordings from CA1 pyramidal neurons are used in most of the illustrations below. The waveforms in Fig. 1C and F give examples of averaged and single traces recorded from a CA3 neuron in an experiment with minimal stimulation of mossy fibres. Note that the single sweeps (Fig. 1F) were selected to illustrate both spontaneous "synaptic noise" (Fig. 1Fa and Fc) and evoked minimal excitatory postsynaptic currents (EPSCs, Fig. 1Fb and Fc). The spontaneous EPSCs can start before the stimulus artefact and thus interfere with the evoked EPSCs (Fig. 1Fb). In the trace c (Fig. 1F) the spontaneous EPSC started apparently before the stimulus and thus the evoked response does not look essentially contaminated by the synaptic noise. However, the measurement of the baseline can be distorted if made just before the stimulus artefact, as it is commonly done.

2.2. Recordings of postsynaptic responses: postsynaptic potentials or currents?

Unitary or minimal postsynaptic responses can be recorded either under voltage or current clamp. Each mode has advantages and disadvantages as reviewed by Jack et al. (1994) and Walmsley (1993). As both reviews stress, in practice the signal-to-noise ratio may be better for the current clamp recordings as compared to the voltage clamp that is important for precise determination of quantal parameters. However, when the response amplitude is large, several problems arise with current clamp recordings. For instance, a reduction in the driving force for the underlying synaptic current or/and activation of potential-dependent

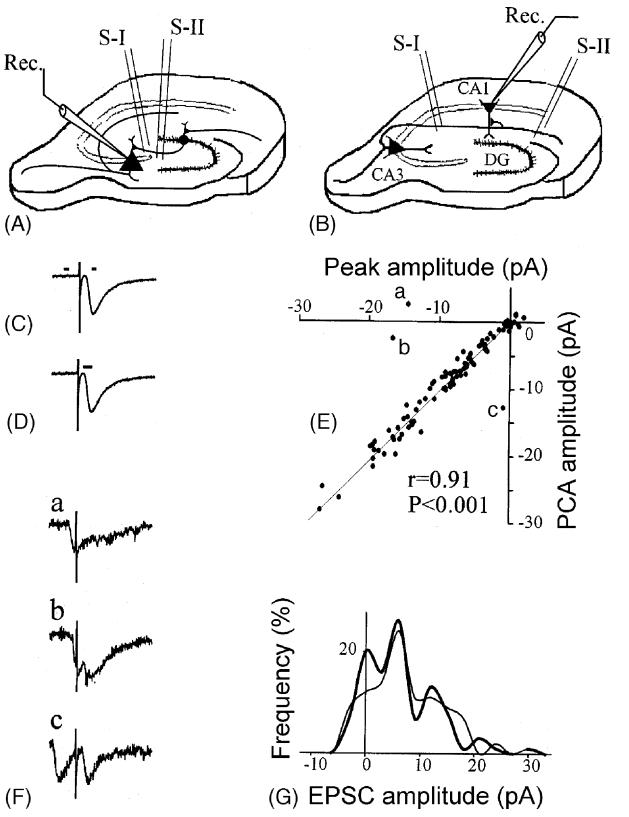

Fig. 1. Recordings and measurements of minimal hippocampal excitatory postsynaptic responses. (A and B) Electrode arrangement in experiments with recordings from CA1 (A) and CA3 pyramidal neurons in the hippocampal slice preparation (B). Recording electrodes (rec.) and electrodes located to stimulate the mossy fibre tract in CA3 and the Schaffer collaterals in CA1 (S-I and S-II) are shown. (C and D) Averaged ($N = 100$) minimal EPSCs recorded from a CA3 neuron. The EPSC is reproduced twice to put the bars that mark the windows for the measurement of the peak amplitude and for the principal component analysis (C and D, respectively). (E) Correlation between the peak amplitudes and the first principal component scores (expressed in pA and called "PCA amplitudes") from the same experiment. The linear regression line, the Pearson correlation coefficient (r) and its significance level (P) are given. Letters a–c mark data points that strongly deviate from the linear correlation and correspond to respective traces in F. (F) Single traces contaminated by spontaneous activity that distorts the peak amplitude measurement but does not essentially influence the PCA amplitude. Traces a and b are taken from the same experiment shown in C and D. Trace c is taken from a different experiment under the same experimental conditions to exemplify a different type of such deviations from the strong correlation between the peak amplitude and PCA amplitude measurements. (G) Amplitude distributions from the same experiment built from the PCA amplitudes and peak amplitudes (thick and thin lines, respectively). Note clearer "quantal" peaks for the PCA amplitudes as compared to the peak amplitudes due to a better signal-to-noise ratio. Altogether E and G show that both measurements give highly correlated and very similar data but with the better signal-to-noise ratio for the measure based on the scores of the first principal component. Here and in all other hippocampal experiments the slices were kept at 32 or 35 °C. $GABA_A$ inhibition was pharmacologically blocked to isolate the minimal EPSCs. See original publications for other details. The recording protocols illustrated in this figure were similar to those of Gasparini et al. (2000). From Voronin, Altinbaev, Bayazitov, Gasparini, Kasyanov, Saviane, Savtchenko and Cherubini (submitted).

channels could lead to non-linear summation of postsynaptic responses. If the effects of non-linearity are thought to be significant, it is preferable to use voltage-clamp mode and to record PSCs rather than PSPs.

The background noise includes the noise due to electrode resistance as well as due to opening and closing of membrane channels, specifically the activity of the channels resulting from ongoing spontaneous and evoked neurotransmitter release ("synaptic noise"). The latter can induce additional complications due to its non-linear interaction with recorded PSPs. To keep the electrode resistance and therefore the noise level to a minimum, whole-cell patch electrodes (Blanton et al., 1989; Edwards et al., 1989) rather than "sharp" microelectrodes have been commonly used for intracellular recordings recently. One disadvantage of the whole-cell recordings is perfusion of the cell with the electrode solution. This can be avoided by using the somewhat more complicated techniques of the "perforated" whole-cell recordings (Horn and Marty, 1988). Development of patch clamp techniques in combination with the optical techniques permitted recordings from thin dendrites of neocortical and hippocampal neurons to be introduced (Benke et al., 1998; Magee and Johnston, 1995; Stuart et al., 1993). Recordings in the close proximity to the synaptically activated dendritic site improves signal-to-noise ratios due to higher amplitude of the postsynaptic signal and gives a better control of the effects of non-linear summation.

2.3. Measurements of postsynaptic responses: peak amplitude and time integral

Having obtained PSPs or PSCs, the next important step before performing quantal analysis is to measure the magnitudes of the recorded events. Various types of amplitude measurements have been tried. The simplest way is to measure the peak amplitude as a difference between two points: at the peak and at the baseline. Normally, the time of the peak is determined from the average waveform and is fixed for measurements of single events. However, some authors use a computer algorithm (or visual guidance) that finds the peak in each individual response. A disadvantage of this procedure is that it can produce amplitude fluctuations not directly related to true "quantal" fluctuations but rather related to "quantization" of the background noise. Such "quantization" can be in part due to the quantal nature of the spontaneous synaptic bombardment, but can also arise from steps in the electronic noise or hum.

One disadvantage of the measurements at a single point is its high variability due to the baseline noise. This can be reduced by averaging over a number of adjacent data points. One approach is using a "mean window amplitude", i.e. an average over a time window covering a part of the PSP/PSC, e.g. initial part of the PSP rising phase (Voronin et al., 1992a). Application of this method has been motivated by observing notches on the rising phase of minimal EPSPs (see e.g. Fig. 4B). The presence of such a notch suggests that the PSP could contain more than one component with different latencies. In such cases, the window can be chosen to cover only the rising phase of the short latency component. However, the measurements of the "mean window amplitude" and the peak at a fixed time point have a disadvantage because the contribution of each monosynaptic quantal component to the recorded PSP does not necessarily occur at the same latency (Walmsley, 1993). Such a "latency jitter" (Barrett and Stevens, 1972) is different in different preparations, sometimes being rather small so it can be neglected. However, it can be essential in synapses with multiple release sites and at low (room) temperature. Therefore some authors claim that "it is not meaningful to use peak amplitude as a measure of synaptic transmission" and recommend "the time integral of the current to obtain the charge" (Bekkers and Stevens, 1991). The charge transfer or the time integral over the entire time course of a postsynaptic response has been used by some groups. However, in practice, it has been shown that this measurement may produce an extremely poor signal-to-noise ratio (Korn and Faber, 1987; Walmsley, 1993). An empirical approach can be used to find the optimum measurement region, i.e. a range of different time windows can be tested intermediate between the whole time integral and single data point. This procedure can be continued until the region producing the best signal-to-noise ratio is chosen (Walmsley, 1993). Typically, the "measurement window" is set around the peak of the average response, while the second ("baseline window") is set before the response onset, e.g. as illustrated by horizontal bars in Fig. 1D. The average value over the baseline window is calculated and subtracted from the average value over the measurement window. As indicated by Walmsley (1993), the choice of a finite time window results in a measure that is neither a peak amplitude nor a complete time integral. To obtain a precise amplitude value, a correction factor should be introduced by dividing the peak amplitude of the average response by the mean value over the chosen window (Walmsley, 1993).

Typically, the time window contains only a few points especially when fast EPSCs are recorded (Fig. 1C). When only a few points are used, the advantage of the averaging is not large because the signal-to-noise ratio increases as the square of the number of averaged signals. To use more full information contained in the response waveform one can use methods based on the multivariate statistical technique of the principal component analysis (PCA). This multivariate technique (Harmon, 1979; Hotelling, 1933; Jackson, 1991) has been applied to CNS studies including brain imaging (see Friston, 1996 for review), artificial neural nets (Churchland and Sejnowski, 1992) and especially electroencephalographic evoked responses (Barth and Di, 1992; Chapman and McCrary, 1995; Glaser and Ruchkin, 1976; Musial et al., 1998). Recently algorithms for application of the PCA to intracellularly recorded EPSPs and EPSCs have been elaborated and used in practice (Astrelin et al., 1998; Berretta et al., 2000; Kasyanov et al., 2000;

Sokolov et al., 2002, 2003; Voronin et al., 1999; see also Henery et al., 1998).

Below we follow two traditional descriptions (formalized and geometrical) of the basis of the PCA as they are used in the above cited handbooks and reviews. The formalized description is mainly in Appendix A to avoid an excess of mathematical formulas in the main text. Additional details can be found in the above cited standard textbooks. Electrophysiological applications of PCA were reviewed by Chapman and McCrary (1995) and Glaser and Ruchkin (1976).

3. Measurements of postsynaptic responses using principal component analysis

3.1. Introduction and simple applications

PCA is a mathematical method that helps to find factors underlying variability of experimental data (Harmon, 1979; Jackson, 1991). We applied a PCA algorithm (Astrelin et al., 1998) to both simulated EPSPs and minimal EPSPs recorded from CA3 and CA1 hippocampal pyramidal cells (see Fig. 1A and B and above cited publications from our group for additional methodological details). The PCA can be described in terms of signal space geometry (Glaser and Ruchkin, 1976; Harmon, 1979). In these terms, postsynaptic responses are first defined in a data signal vector space of T dimensions so that each recorded sweep represents a single vector. In practice, we used $T = 40$–80 so that a window could include a small time region (up to 1.5 ms) before the beginning of the average response, its initial slope and might include its peak. The task of the PCA is to determine if the same data signal vectors could be adequately represented in a subspace of fewer dimensions. Therefore, the principal components represent linear combinations of the original sweeps, which explain successively a maximum amount of response variance and are orthogonal to each other (see Appendix A for equations and more details). In the simplest case, when all postsynaptic responses have the same shape and are different just by a scaling factor, the PCA would reveal that there is one principal component that corresponds to the average postsynaptic response. All information about variability of sweeps would then be provided by the scaling factors (one for each sweep), which are called the scores of the first principal component in terminology of PCA. The score C1 for a sweep is equal to a correlation between the sweep and the first principal component multiplied by the ratio between the standard deviations of the sweep and the first principal component. The score can be normalized to the peak amplitude to be expressed in the units of the voltage (mV) or current (pA). Here, we refer to such score-derived amplitudes as "PCA amplitudes". The procedure of the normalization is analogous to that described above for the normalization of the amplitudes obtained over a window around a peak.

Our data show that the first component scores usually strongly correlate with the most commonly used peak amplitude measurement, giving most of the measurements as equal within the noise level (Fig. 1E). The coefficient of the correlation is always high (>0.85, often >0.9) and highly significant as exemplified by Fig. 1E ($r = 0.91$, $P < 0.001$ at $N = 100$). The question arises, why use such a sophisticated measurement method if the correlation with the measurements of the peak amplitude is so high and thus the mean output provided by both methods should be the same, as has been confirmed (Voronin et al., 1999 and our unpublished observations). There are several reasons that make this method of measurement advantageous. First of all, PCA uses all information contained in a larger window as compared to the peak amplitude measurement, but in distinction from the charge transfer it does not decrease but rather increases the signal-to-noise ratio. The amplitude distribution built from PCA amplitudes is clearly more "peaky" in Fig. 1G than that obtained using the peak amplitudes (thick and thin lines, respectively) due to the better signal-to-noise ratio. A related advantage is illustrated by considerations of the three data points that show a strong discrepancy between the two measures (Fig. 1Ea–Ec). Respective single sweeps (Fig. 1F) indicate that the reason for the discrepancy is contamination of the evoked EPSCs by occasional spontaneous activity. Importantly, the "PCA amplitudes" gave more reasonable values, e.g. a small negative value comparable to the noise level (Fig. 1Ea) for the trace shown in Fig. 1Fa, unlike the peak amplitude measurement that gave rather large amplitude (about −14 pA). In practice, such contaminated sweeps can be discarded following a visual inspection or measured again with a different baseline window. However, visual inspection becomes impractical when hundreds of sweeps are recorded. The comparison of the two measures (Fig. 1E) quickly indicates such "doubtful cases" that can be taken for visual inspection if a researcher prefers peak amplitude measurements. We note that there is no need to discard similar sweeps when the PCA amplitude is used. In distinction from the peak amplitude, the latter measure uses only one window rather than two. It is well known that generally, an error increases when differences between two variable measures are used.

To better understand PCA outcome, simulation experiments were performed (Astrelin et al., 1998). The waveform of simulated EPSPs was described by a function of time using two exponentials: $E(t) = A[\exp(-t/T_{\text{decay}}) - \exp(-t/T_{\text{rise}})]$, where amplitudes A were uniformly or normally distributed. The waveforms were convolved with a Gaussian noise. The standard deviation (S.D.) of the noise (S_n) was varied in different experiments giving different signal-to-noise ratios. Either non-quantal (continuously distributed) or "quantal" EPSPs were simulated. For the latter, the number of release sites (n) was taken to be 1 or 2. The release probability (p) was usually set at 0.5, so that either about 50% ($n = 1$) or 25% ($n = 2$) of the waveforms represented transmission failures with zero mean and S.D. equal

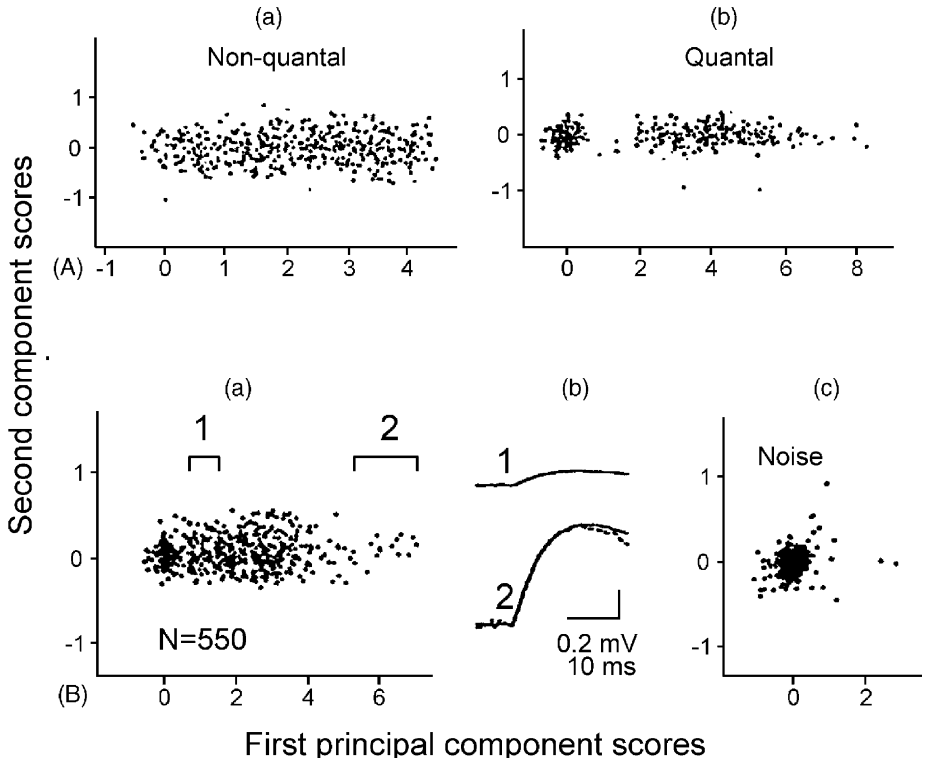

Fig. 2. Principal component analysis of simulated waveforms with one component (A) and its comparison with a plot from a hippocampal minimal EPSP (B). (A) Plots of the first against second component scores (C2/C1 plots) obtained from simulated non-quantal (Aa) and quantal waveforms with one component (Ab). (B) Similar plots obtained from a minimal EPSP recorded from a CA1 pyramidal cell (a and b) and from baseline noise measurements (c). Note band-like plots for both simulated monocomponent EPSPs (A) and for the real EPSP in this particular case (B). Numbers 1 and 2 in Ba mark regions corresponding to small (presumably monoquantal) and large (multiquantal) responses, respectively. Averages corresponding to the data points from the regions 1 and 2 in Ba are shown in Bb. The dashed curve in Bb2 represents the record Bb1 scaled in such a manner that its peak amplitude matches that of Bb2 to show that the time courses are similar for the EPSPs with a small (region 1 in Ba) and large amplitude EPSPs (region 2 in Ba). The noise measurements (Bc) were obtained from the same sweeps as used for Ba but for prestimulus periods. Note that the width of the Bc plot along the *y*-axis is similar to that in Ba, suggesting the absence of a second component in Ba. Modified from Astrelin et al. (1998).

to S_n. Either "small" (0.15–0.3Q) or large (>Q or >S_n) intrinsic variation of the quantal size (Q) could be added to the non-failures.

Fig. 2A exemplifies principal component scores obtained from simulations of a simple waveform having one component. Noise-contaminated non-quantal (Fig. 2Aa) and quantal EPSPs (Fig. 2Ab) were simulated. The plot of the scores of the second component against the first one ("C2/C1 plot") gave a band with a width that depended on S_n. With a Gaussian noise, about 96% of the values should fall within $\pm 2S_n$ along the *y*-axis. In the case of the quantal EPSPs, transmission failures were represented by a cloud around point (0, 0) (Fig. 2Ab). The cloud was clearly separated from the rest of the data points because of large signal-to-noise ratio used in these simulations. Fig. 2B illustrates a similar plot for an EPSP recorded from a CA1 neuron. Note that the C2/C1 plot (Fig. 2Ba) is similar to that for the simulated monocomponent EPSP (Fig. 2Ab), although the cloud containing transmission failures was not as clearly separated from the rest of data points as in the simulation with a low noise. Nevertheless, the "failure cloud" can be distinguished from the rest of the data points, suggesting the presence of a minimal non-zero increment presumably due to quantal release. The width of the band (Fig. 2Ba) is comparable to the width of the C2/C1 plot for the baseline noise, thus, suggesting the absence of an essential contribution from a second component. Panels b1 and b2 (Fig. 2B) illustrate similar time courses of the scaled averaged responses corresponding to two different regions having small and large response amplitudes, respectively. This is also compatible with the presence of only one component. It was further confirmed by averaging the data points around (0, 0) coordinates that produced no discernable response (not shown, see similar "flat average" in Fig. 4F4).

3.2. Analysis of simulated multicomponent EPSPs

There is one more important advantage of the measurement based on the PCA, that is its ability to separate and measure independently underlying components of a postsynaptic response. Indeed, unitary responses may consist of several components with different latencies and waveforms when a presynaptic fibre establishes several synaptic connections at various electrotonic distances from the recording

site. When "minimal" rather than unitary responses are analyzed, the number of activated presynaptic fibres can be more than one as noted above. Accordingly, the responses can show clear signs of the presence of different components such as notches at the initial slope (Alger et al., 1996; Voronin et al., 1992a), bimodal latency distributions (Edwards et al., 1990; Stern et al., 1992; Torii et al., 1997) and different waveforms for different amplitude ranges (Stricker et al., 1996a, 1996b; Voronin et al., 1996). Quantal analysis based on commonly used measurement methods may give false results in the presence of more than one component. One way to separate different EPSP components is to consider their latencies (Stern et al., 1992; Torii et al., 1997; Voronin et al., 1996). However, the measurements from single trials are not reliable when the latency differences and signal-to-noise ratios are small. A better separation may be achieved using full information contained in both response latencies and waveforms. This is provided by the PCA.

While the meaning of the first PCA component in case of minimal postsynaptic responses is very clear, as explained above, the interpretation becomes more difficult when several components are present. To obtain a meaningful interpretation of the basic waveforms and their scores, several procedures can be used, most popular being "varimax rotation" (Glaser and Ruchkin, 1976; Harmon, 1979; Jackson, 1991). These procedures produce new "components" that may be useful although they are obtained by different criteria from PCA. We elaborated and tested a graphical procedure suitable for minimal EPSPs. The procedure was called "alignment" (Astrelin et al., 1998, see also Appendix A, Section 3). We shall illustrate it using simulated bicomponent EPSPs (Fig. 3) and physiological recordings (Figs. 4, 6 and 7C).

To simulate two components, different time constants or latencies were introduced to obtain two simulated waveforms (Fig. 3Aa, two upper traces). Afterwards, the two waveforms were mixed so that the sample (typically $N = 500$) consisted of bicomponent waveforms (Fig. 3Aa, mixture), monocomponent waveforms and failures. A Gaussian noise was added to the simulated waveforms (Fig. 3Ab). The aims of the simulations were to test PCA algorithms, to assist elaboration of the alignment procedure and to facilitate interpretation of the components obtained in the physiological experiments.

As the first step of the algorithm implementation, a window was defined as described above. After this, the program calculated PCA scores (see Appendix A) and showed them as two-dimensional plots (Fig. 3B). The illustrated simulation experiment produced plots of the scores of the first (C1) and second (C2) principal components as a parallelogram with an apex at (0, 0) which was typical for bicomponent simulations. The next step was to consider similar plots for later (C3–C8) components. In this experiment, the C3/C1 plot (Fig. 3Ca) represented a band with the width comparable to that of the noise indicating the absence of C3 (see Appendix A, Section 2). The C4/C3 plot (Fig. 3Cb)

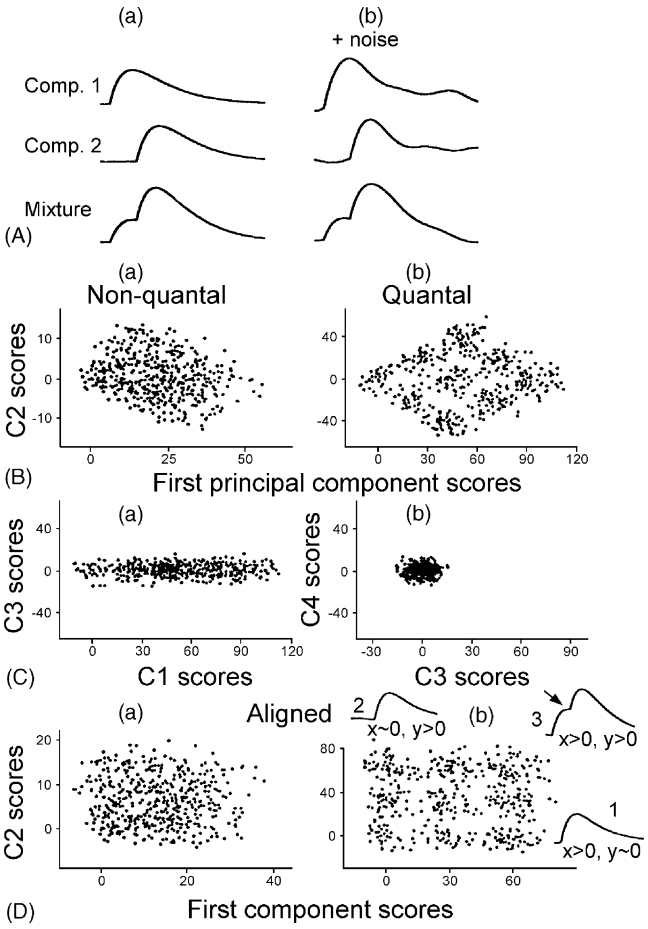

Fig. 3. Component analysis of simulated bicomponent waveforms. (A) Simulated waveforms with shorter (comp. 1) and longer (comp. 2) latencies, their mixture (column a) and the same waveforms contaminated with noise (column b). Two waveforms with different latencies and with response failures were simulated and mixed. Either non-quantal or quantal release with two release sites was assumed. (B) Plot of the scores of the two initial principal components from experiments with simulations of non-quantal (a) and quantal (b) waveforms. Note characteristic parallelograms suggesting the presence of two components. (C) The scores of the third principal component plotted against the first (a) and the fourth (b) ones. Note the narrow band (a) and the cloud (b) suggesting that the third and fourth components were absent. (D) Alignment procedure and extraction of the simulated waveforms; a and b present transformed ("aligned") plots of Ba and Bb, respectively. Note that the parallelograms shown in B were transformed into rectangular fields. Insets (1–3) show waveforms obtained by averaging the simulations corresponding to the dots from different parts of the plots in b: (1) for the band along the x-axis with y values $0 \pm 2S_n$; (2) for the band along the y-axis with x values within $0 \pm 2S_n$; (3) for the cloud with both x and $y > 2S_n$. Note that the procedure restores the waveforms (Db1–b3) identical to the simulated ones (A). The arrow (Db3) marks the notch corresponding to the beginning of the longer latency component. Five hundred waveforms were simulated in each of the simulation experiments shown here and in other figures. From Astrelin et al. (1998).

was practically indistinguishable from the noise plot. Bands similar to Fig. 3Ca were observed for other combinations of C1 or C2 with later components (not illustrated) and the noise clouds similar to Fig. 3Cb were observed for other

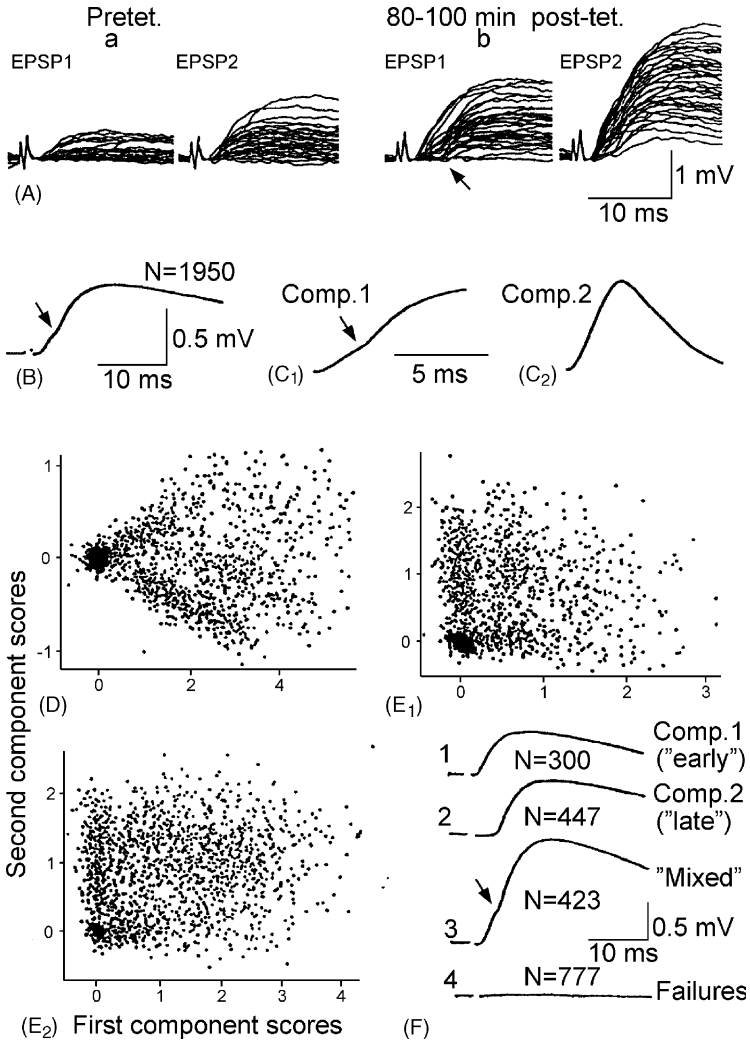

Fig. 4. Minimal hippocampal EPSPs (A and B) and their component analysis (C–F). (A) Superposition of consecutive single responses ($N = 50$) recorded from a CA1 pyramidal neuron before (pretet.) and after (post-tet.) conditioning tetanic stimulation. Responses to the first (EPSP1) and second (EPSP2) stimuli in the paired-pulse paradigm are shown. The resting membrane potential was −61 mV in the beginning and −64 mV at the end of the experiment; the input resistance was 157 and 132 MΩ, respectively. The small changes in either the membrane potential or input resistance did not correlate with the amplitude changes. (B) Average waveform of all recorded EPSP1. The arrow marks a notch on the rising phase suggesting existence of two components. (C and D) First (C1) and second (C2) principal components and their scores (D) obtained after standard PCA. (E) Scores of two initial components for EPSP1 (E1) and EPSP2 (E2) after the alignment procedure (Section 3.2). Note the rectangular shape of the plots with gaps suggesting existence of separate (and quantal) components (compare with simulated data of Figs. 3Db and 5Bb). (F) Separation of pure components of EPSP1 using the averaging procedure analogous to that illustrated in Fig. 3Db. According to the results of this procedure, the responses associated with dots along the *x*-axis (1) and *y*-axis (2) appeared to represent short- and long-latency components, respectively. The row 3 represents their mixture that is similar to the average of all sweeps in B (arrow marks a notch on the rising phase). The row 4 represents the average of the trials corresponding to the cloud around the coordinates (0, 0) in E1 (transmission failures). From Astrelin et al. (1998).

PCA components, which were not simulated in this particular experiment. Summarizing, the above considerations of the component plots were in agreement with the simulation of bicomponent EPSPs.

The next step was the alignment of the visually inspected C2/C1 plots. We used a computer algorithm that is described in Appendix A. Briefly, the plot was aligned in such a way that the borders of the parallelogram became parallel to the ordinate and abscissa axes. The result of such alignment of Fig. 3Ba is shown in Fig. 3Da. It gave a rectangular plot typical for bicomponent cases. Fig. 3Bb illustrates simulations with two quantal levels and small quantal variance. The "quantization" did not change general shapes of the plot, except for the separation of the cloud of failures around the coordinate (0, 0). Nevertheless, it essentially facilitated the alignment due to gaps and additional borders (Fig. 3D, compare a and b).

The aligned plots were used to interpret the meaning of the components and to "restore" the simulated waveforms. To this aim we averaged the waveforms, which corresponded to positive scores for a given coordinate and about 0 scores (within $\pm 2S_n$) for the second coordinate (Fig. 3Db, insets 1

and 2). For example, Fig. 3Db1 was obtained by averaging the waveforms corresponding to the dots along the *x*-axis with *y* values close to 0. Similarly, Fig. 3Db2 was obtained by averaging all responses corresponding to the dots along the *y*-axis with first component scores near zero. The recovered components (Fig. 3Db1 and Db2) were identical to the simulated waveforms with different latencies (Fig. 3Aa). Accordingly, the averaging of the simulations corresponding to both *x* and *y* positive (Fig. 3Db3) was identical to the mixture of the simulated components (Fig. 3Aa). The inflection point (Fig. 3Db3, arrow) corresponded to the beginning of the longer latency component.

3.3. Comparison of simulation and physiological experiments: components with different latencies and rise times

Cases with two components different in their latencies were most commonly encountered in physiological experiments (see summary in Fig. 8). Fig. 4A illustrates EPSPs recorded from a CA1 neuron with paired-pulse testing stimulation before and after conditioning afferent tetanization was delivered following 300 initial testing pairs (see Sokolov et al., 2002 for methodological details). Comparisons of the first and second EPSPs (EPSP1 and EPSP2, respectively, in Fig. 4A) show typical paired-pulse facilitation (PPF). LTP was evident as a strong increase in the EPSP1 amplitude (Fig. 4A, post-tet.) with reduction in the number of transmission failures (N_0). The latency of the averaged response (Fig. 4B) was 2.3 ms, but the consideration of both single and averaged responses revealed a component with a longer (5.4 ms) latency (Fig. 4A and B, arrows). Panels C–E illustrate consecutive steps of the PCA that led to separation of the components with different latencies and identification of their waveforms.

Fig. 4C1 represents the new basic waveform revealed by the PCA. It is commonly termed first principal component (f_{1t} from Eq. (A.2) in Appendix A) and reflects essential features of the initial part of the average EPSP (Fig. 4B) taken for the analysis. The meaning of the second principal component (f_{2t} in Appendix A) shown in Fig. 4C2 was more difficult to interpret. Therefore as the next step, the alignment of the initial C2/C1 plot (Fig. 4D) was used to obtain interpretable results. The shape of Fig. 4D (parallelogram with clear borders similar to Fig. 3Bb) suggested a good component separation. Accordingly, there was no difficulty to perform the alignment, and the aligned plot (Fig. 4E1) appeared to be similar to the simulated plots with quantal components (Fig. 3Db). The analogous plot for EPSP2 (Fig. 4E2) showed a smaller cloud around (0, 0) as compared to Fig. 4E1, reflecting PPF. To obtain the waveform of the new first component (comp. 1 in Fig. 4F) that appeared as a result of the alignment, we followed the procedure of Section 3.2 and averaged the waveforms corresponding to the dots along *x*-axis in Fig. 4E1. Analogous procedure was performed to obtain C2 (Fig. 4F, comp. 2). C1 and C2 (Fig. 4F1 and F2) appeared to be alike in their waveforms but their latencies differed (2.3 and 5.4 ms, respectively). The responses from the cloud with positive *x* and *y* values in Fig. 4E1 could be interpreted as mixtures of the early and late components. Accordingly, their average (Fig. 4F3) was similar to the general average (Fig. 4A) and contained a notch (Fig. 4F3, arrow) corresponding to the expected transition between the two components. The average response (Fig. 4F4) corresponding to the cloud around 0 in Fig. 4E1 confirmed that this cloud represented mostly failures and indicates the absence of additional independent components.

Fig. 5 illustrates non-aligned (a) and aligned plots (b) obtained with simulations of two components having the same latency but different kinetics. The non-quantal and quantal cases (Fig. 5A and B, respectively) further illustrate that the latter is easier to align along the axes due to additional gaps and borders. Insets 1–3 (Fig. 5Bb) give the results of the recovery of the simulated components with the fast (Fig. 5Bb1) and slow (Fig. 5Bb2) rise times (T_{rise}) as well as their mixture (Fig. 5Bb3) using the procedure of Section 3.2. The component waveforms shown in Fig. 5Bb were equivalent to actually simulated waveforms similar to those in Fig. 3A but with different kinetics rather than latencies.

A hippocampal EPSP having two components with different kinetics but similar latencies is illustrated in Fig. 6A. The average waveforms associated with the data points along the *x*- and *y*-axes are given in Fig. 6C1 and C2, respectively. Since their T_{rise} differed they were termed “slow” and “fast”, respectively. Fig. 6D and E illustrate changes of their scores during the experiment with LTP induction. Note similar time courses for the respective components of EPSP1 and EPSP2 but different changes of the slow and fast components, suggesting their association with different synapses. It is noteworthy that different components contributed differently to earlier and later LTP phases. There were practically no positive scores for the EPSP1 of the fast component before tetanus (Fig. 6E1), so that it represented a “virtually silent” synapse prior to LTP induction. Appearance of occasional positive scores of the EPSP2 of the same component before tetanus (Fig. 6E2) indicates that the synapse was “presynaptically silent” (Gasparini et al., 2000; Torii et al., 1997; Voronin and Cherubini, 2003) rather than “postsynaptically silent” (Durand et al., 1996; Isaac et al., 1995; Luscher and Frerking, 2001). Finally, we note that after LTP induction the fast component behaved in an “all-or-none” mode (Fig. 6E1 and E2) so that mostly failures and large amplitudes appeared while the number of intermediate responses was small. In this respect they were similar to neocortical EPSPs presumably recorded from large thalamo-cortical synapses (Stratford et al., 1996; Volgushev et al., 1995).

3.4. Comparison of computer simulations and physiological data: variable waveforms

We tested whether it is possible to distinguish between postsynaptic responses containing two components from a

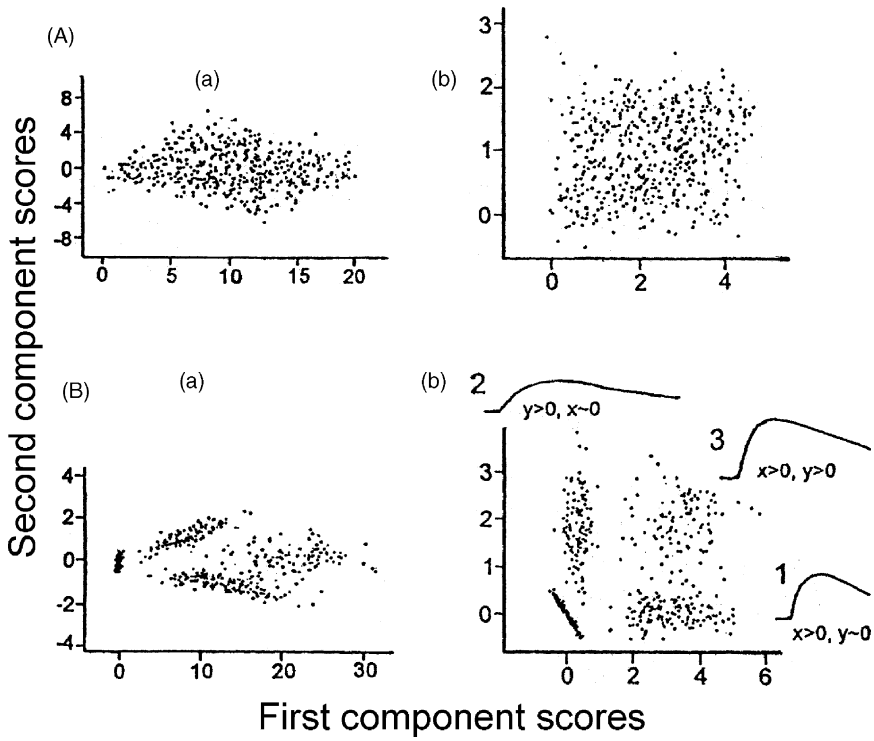

Fig. 5. "Alignment" of the PCA scores and extraction of the simulated waveforms in experiments with simulations of two components having the same latencies but different kinetics. (A and B) Non-quantal and monoquantal EPSPs were simulated, respectively. The plots are shown before (a) and after their alignment along the axes (b). Note that the parallelograms (a) were transformed into rectangulars after the alignment procedure (b). Insets 1–3 in Bb show waveforms obtained by averaging the waveforms corresponding to different parts of the plots (see Fig. 3 legend for more details). The averages 1 and 2 were identical to the simulated components with different kinetics; the inset 3 represents the mixture of 1 and 2. Modified from Astrelin et al. (1998).

continuum of variable waveforms. Fig. 7A and B illustrate C2/C1 plots from simulations of non-quantal and quantal variable waveforms, respectively. This could imitate activation of a continuum of different presynaptic fibres with different kinetics of respective PSPs. Such plots were difficult to align, especially with small N (<200) and large noise ($Q/S_n < 2$), due to less clear a border than that of the bicomponent plots (Fig. 2B). The alignment produced C2/C1 plots (Fig. 7Ab and Bb) with a negative correlation between the components and with a shape close to a triangle rather than to a rectangle. The star in Fig. 7Ab denotes the blank region without cases with large C1 and C2 scores. This is in agreement with the fact that no sum of components was simulated. The averaging procedure of Section 3.2 resulted in the appearance of waveforms with different kinetics (Fig. 7B1–B3). The result agrees with the simulation of waveforms that varied between those in Fig. 7B1 and B3. However, by itself it did not allow to decide whether the initial data (Fig. 7Ab) contained discrete components or represented a continuum of variable waveforms. Our simulations showed that to answer this question, one should first analyze the C2/C1 plots (Fig. 7Aa and Ba) and to try to align them (Fig. 7Ab and Bb). Rectangular plots without correlations (e.g. Fig. 5Ab and Bb) would indicate the presence of discrete components, whereas a triangle structure with a blank sector (Fig. 7Ab, star) would suggest waveform variations.

Fig. 7C illustrates data obtained from physiological recordings that presumably reflect EPSPs with waveform variations. Both initial (Fig. 7Ca) and aligned (Fig. 7Cb) C2/C1 plots had structures typical for the simulations of variable waveforms (compare with Fig. 7Ba and Bb, respectively). The averages corresponding to the EPSPs with amplitudes along the x-, y-axis and the intermediate region (Fig. 7Cb1–b3, respectively) suggest either strong waveform variations in one input or activation of a large number of presynaptic axons producing EPSPs with different T_{rise}.

The simulations of the variable waveforms (Fig. 7A and B) imitate also cases with a large number of different components, each appearing with a low probability. When >2 independent components were simulated, the initial C2/C1 plot had a more complicated shape as compared to the parallelograms of the bicomponent plots (see Astrelin et al., 1998 for illustrations and more details). For example, the plot represented a hexagon- or an octagon-like field for three or four simulated components, respectively. The absence of clear borders made the alignment difficult. It was possible to perform the alignment only at high Q/S_n (>2.5) with clear quantal groupings. At lower Q/S_n or non-quantal simulations, considerations of the plots of different PCA components typically indicated the presence of >2 simulated components, but their separation was not possible. One

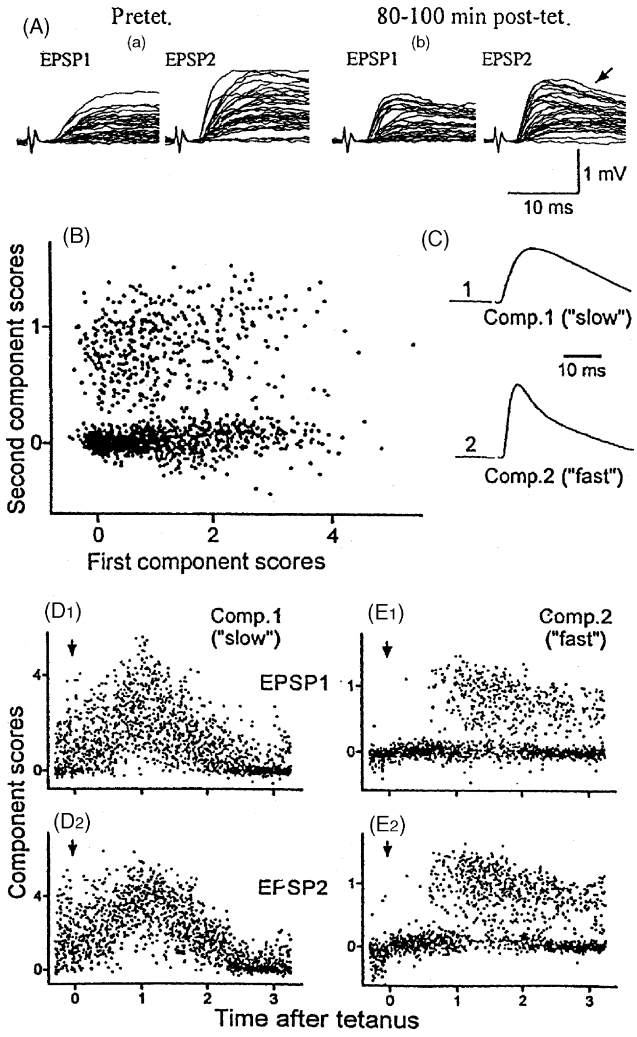

Fig. 6. Minimal hippocampal EPSPs (A) and their component analysis (B–E) resulting in separation of two components with the same latency. (A) Superimposed EPSPs induced by paired-pulse stimulation in a CA1 pyramidal neuron before and after tetanus, as in Fig. 4A. The membrane potential was −62 mV in the beginning and −65 mV at the end of the experiment, the input resistance was 148 and 122 MΩ, respectively. (B) Plot of the scores of two initial components after the alignment procedure. (C) "Pure" first (C1) and second (C2) components obtained by averaging the responses associated with dots located in B along the *x*- and *y*-axis, respectively. Note similar latencies but different kinetics of the "slow" and "fast" components. (D and E) Scores of the first (D) and second (E) components plotted against time for EPSP1 (1) and EPSP2 (2). The arrow marks tetanization. Note similar potentiation time courses for the respective components of EPSP1 and EPSP2, but different changes for different components, suggesting their association with different synapses. From Astrelin et al. (1998).

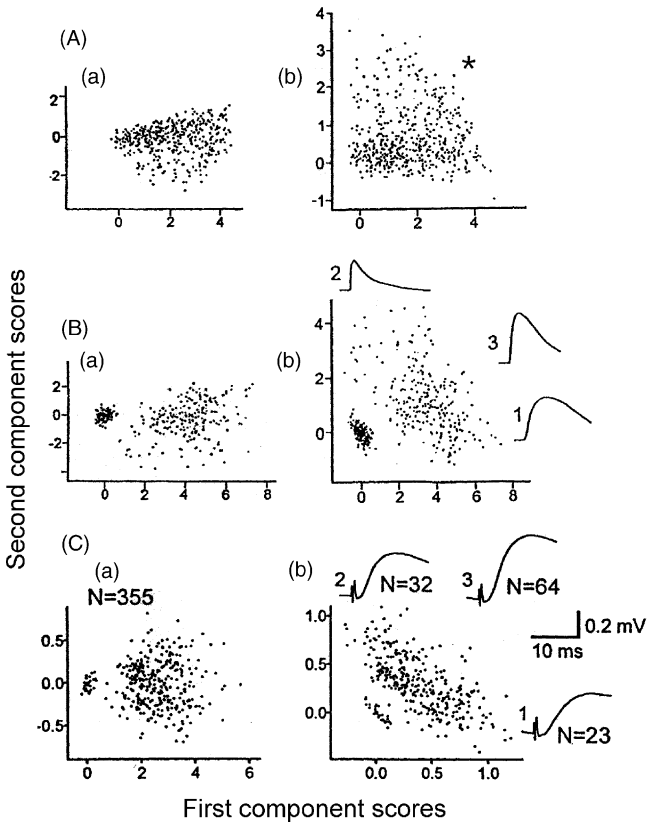

Fig. 7. Comparison of plots of component scores from simulated variable waveforms and from "real" EPSPs giving a similar C2/C1 plot. (A and B) C2/C1 plots from two computer experiments with simulation of non-quantal (A) and quantal (B) variable waveforms mimicking activation of a continuum of different presynaptic fibres with different kinetic characteristics of respective synapses. (C) C2/C1 plots from EPSPs recorded from a CA1 pyramidal neuron. Columns a and b in A–C represent initial PCA scores and component scores obtained after alignment procedure, respectively. Note "fan"-like plots (a) and triangle-like plots (b) obtained from both simulated and physiological experiments. The meaning of 1–3 in Bb and Cb is the same as in Fig. 3Db. The star in Bb denotes the blank region without cases with large C1 and C2 scores. This agrees with the fact that no independent components were simulated. Note similar blank region in Cb indicating that this recording also reflects appearance of multiple EPSPs with variable waveforms. Modified from Astrelin et al. (1998).

characteristic difference from the bicomponent simulations was the presence of clear responses when the trials corresponding to data points at about (0, 0) coordinates were averaged. Our algorithm included an option for the averaging in a multidimensional space. In addition to the high Q/S_n, a sufficiently high number of failures (N_0) for each component was necessary for the complete component separation using this option. However, the cases with plots that could be interpreted as the presence of >3 components were rather exceptional in our physiological experiments (see Fig. 8).

3.5. Limits of the resolution of the components and composition of the recorded minimal EPSPs

Limits of the resolution were explored in over 60 simulations of variable signal-to-noise ratios (Q/S_n), T_{rise} and latencies (see Astrelin et al., 1998 for illustrations and more details). One essential result was that the ratio between the latency difference (ΔL) and the rise time ($\Delta L/T_{rise}$) is a more important variable for separation of two components than is ΔL itself. Fig. 8A–C (open symbols) summarizes the results of our simulations. The ordinates present the normalized C2 width in initial (non-aligned) C2/C1 plots. The dashed line

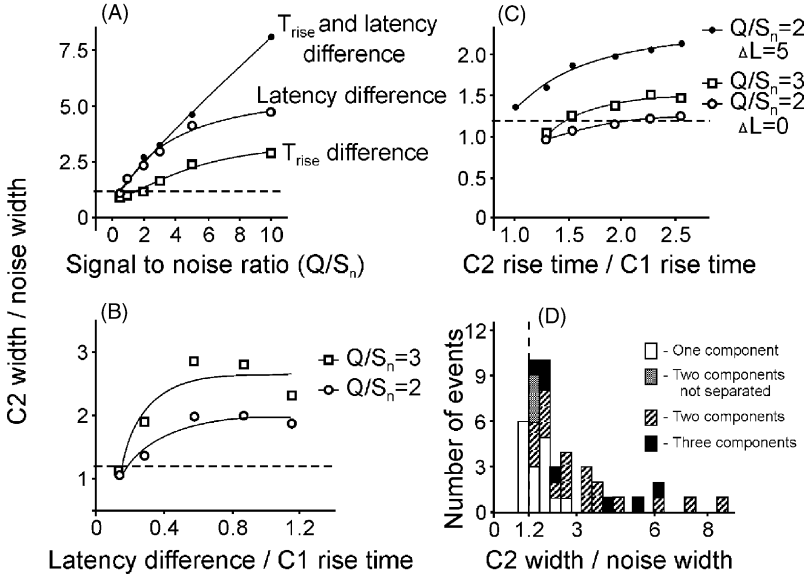

Fig. 8. Summary of the studies on the resolution of the component analysis in simulation (A–C) and physiological (D) experiments. (A–C) Relative width of the second component (C2) in C2/C1 graphs was plotted against signal-to-noise ratios (A); relative latency differences (B) and relative rise times (T_{rise}) of the second component (C). The relative C2 width is determined as the ratio of the width of the second component in C2/C1 graphs to that of the background noise. The latency (B) and T_{rise} (C) differences were expressed as their ratios to T_{rise} of the first component. Monoquantal components were simulated with the binomial parameter $p = 0.5$ and various Q/S_n. Different symbols in A represent simulations with $\Delta L/T_{rise} = 0.9$ (circles), with ratios of T_{rise} of two components equal to 2.5 (squares) and also with $\Delta L/T_{rise} = 0.9$ and in addition with ratios of T_{rise} of two components equal to 2.5 (dots). Rise times or latencies were fixed in the experiments shown in B or C, respectively. (D) Distribution of the relative C2 width in physiological experiments. The dashed lines in A–D indicates the threshold value 1.2 (see Appendix A) for selection of plots with reliable and unreliable component separation. For the cases to the left of the dashed line, components cannot be separated due to too high noise levels. EPSPs with different number of components are shown by different bars as explained in the inset in D. From Astrelin et al. (1998).

marks the C2 width equal to 1.2 at which the component resolution became unreliable (see Appendix A, Section 2). Comparisons of circles and squares in Fig. 8A–C show that the analysis is more sensitive to latency as compared to T_{rise} differences. Thus, at equal latencies, only components with several-fold differences in T_{rise} could be resolved at $Q/S_n = 2$ (Fig. 8C, circles above the dashed line). At equal T_{rise}, small relative latency differences could be resolved even at smaller Q/S_n (Fig. 8B). It should be stressed that Fig. 8A–C represents simulations of monoquantal responses and therefore it evaluates the lower limits of the algorithm resolution. The algorithm became essentially more sensitive when both latency and T_{rise} were different (Fig. 8A and C, dots), which is the most common case in real physiological experiments (Fig. 8D).

The algorithm was applied to analyze recordings of 45 minimal EPSPs ($N = 300$–2200). Fig. 8D summarizes the distribution of the ratios between the width (taken as 2S.D.) of the second component and that of the noise ($2S_n$). The value of the ratio equal to 1.2 was taken as a criterion for reliable resolution of two components (see Appendix A). It is marked by the vertical dashed line. Fig. 8D shows that in six cases (the bar to the left of the dashed line) the width of C2 in the C2/C1 plot was close to that of the noise plot (as in Fig. 2B). Comparison with the plot of the simulated monocomponent EPSP (Fig. 2Ab) and additional analyses (see Section 3.2) including averaging putative failures supported the existence of only one component for these six cases.

The open bars to the right of the dashed line in Fig. 8D correspond to 10 cases with C2/C1 plots (Fig. 3C) having appearances typical for the simulations of variable waveforms. Such plots suggest either strong waveform variations in one input or activation of a large number of presynaptic axons giving EPSPs with different T_{rise}. In 6 out of the 10 cases, latency variations (for 1–3 ms) were also evident.

The grey bars in Fig. 8D correspond to three cases with plots without clear borders, which could not be reliably aligned. Nevertheless, using the strategy elaborated in the simulation experiments it was possible to distinguish these cases from the waveform variation and detect two components. The components differed in their latencies (for 1, 3 ms) and T_{rise} (for 5, 6 and 1.5 ms, respectively, for these three cases). However, our simulations showed that the scores of the individual components can be used only cautiously for further statistical analysis in such cases.

The hatched and black bars in Fig. 8D represent the most numerous group with two ($N = 19$) or three ($N = 7$) distinct components. The components differed either in the latency or T_{rise} (see Figs. 4 and 6, respectively) or both. Altogether, comparisons of all 40 component pairs of this group gave eight cases with different (for 0.8–3.0 ms) latencies,

but with T_{rise} similar within <1 ms (Fig. 4) which was close to the confidence interval for T_{rise}. The latter varied from 4 to 9 ms (6.6 ± 1.9 ms, $N = 8$; mean ± S.D.), which gave the $\Delta L/T_{rise}$ ratios from 0.15 to 0.67 (0.36 ± 0.19). In five pairs, the components differed in T_{rise} for 3–6 ms (5.2 ± 1.3 ms) without any latency differences within the precision of measurements (0.2 ms). The latencies varied from 2.4 to 5.0 ms (3.5 ± 1.0 ms, $N = 5$). Twenty-seven out of 40 pairs showed differences in both latencies (from 0.6 to 7.8 ms; 2.5 ± 1.8 ms) and T_{rise} (from 1.6 to 5.0 ms; 3.8 ± 1.7 ms). As noted above, the differences in both latencies and T_{rise} facilitated the identification of distinct components.

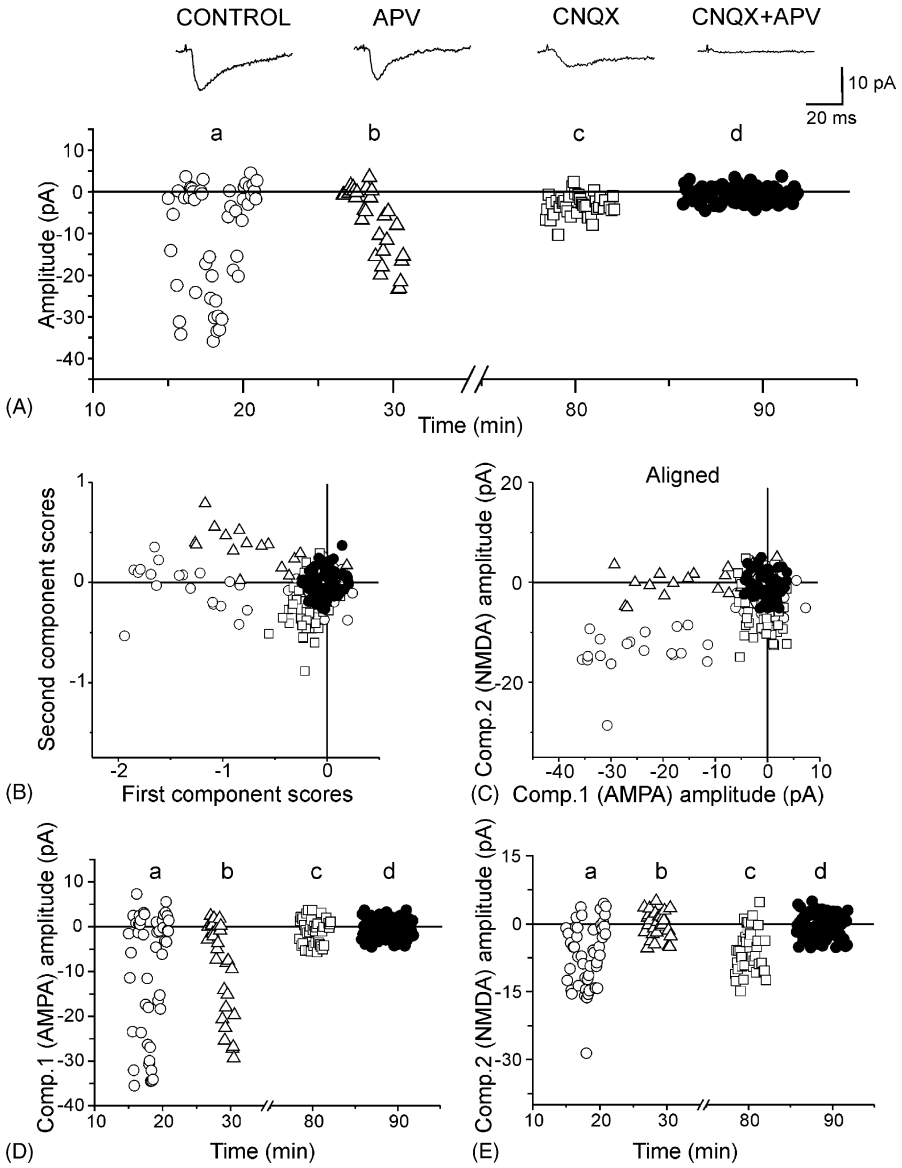

Fig. 9. Combination of the component analysis with pharmacological isolation of EPSC components mediated by glutamate receptors of AMPA and NMDA types. (A) Plot of the amplitudes of EPSCs recorded from a CA1 neuron under control conditions (a) with application of an antagonist of the NMDA receptors (APV, b), of an antagonist of AMPA receptors after APV washout (CNQX, c) and of both receptor blockers (CNQX + APV, d). The waveforms show respective averages of 29–71 trials. Initial periods of the blocker application and the period of APV washout were omitted for clarity. (B) Initial (non-aligned) C2/C1 plot from the same experiment. Different symbols here and in C–E correspond to different periods (a–d) shown in A. (C) The same plot shown in B after its alignment. Note that data points corresponding to pure (pharmacologically isolated) AMPA receptor-mediated responses (triangles) are located along the abscissa, whereas NMDA receptor-mediated responses (squares) are located along the ordinate. (D and E) Plots of the amplitudes of the first (AMPA receptor-mediated) and second (NMDA receptor-mediated) components (D and E, respectively) during the course of the experiment. EPSCs recorded from a CA1 pyramidal neuron under conditions favorable for expression of both AMPA receptor- and NMDA receptor-mediated EPSCs (at −50 mV holding potential with addition of 2 μM glycine to the extracellular solution); APV and CNQX were added at 25 and 0.3 μM concentration, respectively. See Bayazitov et al. (2002) for other methodological details. From Bayazitov, Kleschevnikov and Voronin (in preparation).

3.6. Combination of component and pharmacological analyses

When two (or more) response components are present at the same proportion in every trial, the components cannot be separated because the response is treated as a single identity. Recently we combined the component analysis with a pharmacological approach. We isolated EPSC components mediated by two types of glutamate receptors: α-amino-3-hydroxy-5-methyl-4-isoxazole propionic acid and *N*-methyl-D-aspartate types (AMPA and NMDA types, respectively). Afterwards, we used the pharmacologically isolated "pure" components for the alignment procedure with the final aim to quantify a contribution of AMPA and NMDA receptor-mediated EPSCs to each dual-component postsynaptic response. Fig. 9Aa presents average waveforms and amplitudes of EPSCs recorded from a CA1 pyramidal neuron under conditions favorable for expression of both AMPA and NMDA receptor-mediated EPSCs (holding potential of −50 mV and added glycine). Note that similar to those in Fig. 1, the values in Fig. 9 are negative because they reflect negative-going EPSCs recorded under voltage clamp conditions rather than positive-going EPSPs as in most of other figures. To isolate AMPA or NMDA receptor-mediated components, respective specific blockers were added extracellularly: D-2-amino-5-phosphonovalerate (APV, Fig. 9Ab) or 6-cyano-7-nitroquinoxaline-2,3-dione (CNQX, Fig. 9Ac). The averages of the pharmacologically isolated components and respective response amplitudes are shown in panels b and c of Fig. 9A. Initial periods of the antagonists' applications and a period of APV washout are omitted for clarity. Part d represents an experimental period with simultaneous action of both blockers. Fig. 9B shows an initial (non-aligned) C2/C1 plot. Note that the control response obtained without blockers (open circles) produces a band similar to monocomponent cases while the general plot represents a parallelogram typical for bicomponent cases. Fig. 9C shows the C2/C1 plot after its alignment. Data points corresponding to pharmacologically isolated AMPA receptor-mediated responses (triangles) were aligned along the abscissa whereas NMDA receptor-mediated responses (squares) were aligned along the ordinate. As a result, control EPSCs (open circles) appeared to be found at the usual place of mixed responses (compare with inset 3 in Fig. 3D). Note also that data points corresponding to the application of both blockers (closed circles) overlap with data points corresponding to transmission failures during other experimental periods. Thus, this approach allowed us to plot separately time courses of amplitudes of AMPA and NMDA receptor-mediated components during this experiment (Fig. 9D and E, respectively). Notably, during the periods of CNQX action the amplitudes of the AMPA receptor-mediated component were comparable to the noise level (Fig. 9Dc), supporting correct measurement of the contribution of this component. Analogously, during the period of APV action (Fig. 9Eb) the amplitudes of the NMDA receptor-mediated component fluctuated around zero level as well. In practice, it appeared that application of only one blocker was sufficient for reliable extraction of both components. Using this method we found approximately equal changes of AMPA and NMDA receptor-mediated PSCs recorded from CA1 pyramidal neurons over a period from about 5 min to 2 h after LTP induction (Bayazitov et al., 2002). We stress that this approach allowed us to measure amplitudes of both components in parallel within the same time window after the stimulus and under the same conditions before and after afferent tetanus.

4. Spectral analysis

4.1. Significance of peaks in amplitude distributions and spectral estimate of quantal size

If neurotransmitter is released in a quantal manner, individual responses are evoked by different number of quanta liberated. If quanta are of the same size *Q*, the amplitudes of postsynaptic responses would fluctuate in steps equal to *Q*. When S_n is low enough, several equidistantly separated peaks are expected to be seen in the PSC/PSP amplitude distribution, as shown in Fig. 10A. Therefore, the next step after response measurement could be an analysis of distributions of their amplitudes. A question that arises is whether the peaks in a distribution are meaningful and represent quantal fluctuations of a postsynaptic response under study or if they appeared by chance, due to a limited sample size. The problem is illustrated by Fig. 10B, where the underlying theoretical distribution used to simulate a set of 200 amplitudes was without peaks, but several quasi-quantal peaks are distinguishable in the amplitude distribution reconstructed from simulated data.

Several methods have been introduced to evaluate whether peaks in an experimental distribution are random or reflect

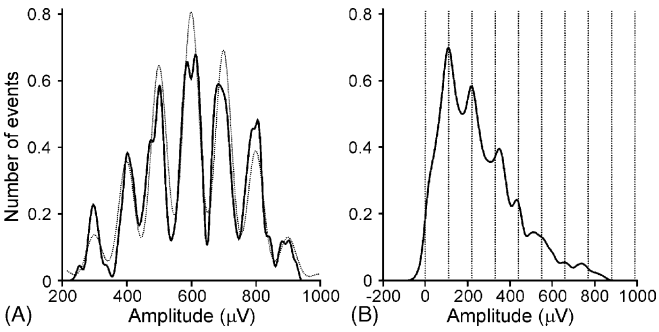

Fig. 10. Simulated amplitude distributions. (A) Mixture of Gaussian distributions separated by 100 μV and S_n = 25 μV was used to simulate 200 amplitudes. The simulated distribution is shown as a solid line, the underlying theoretical distribution is shown as a dotted line. (B) An example of a "peaky" distribution that appeared due to a small sample size. Chi-square distribution was used to simulate 200 amplitudes. Vertical dotted lines are placed with 100 μV interval to indicate "quasi-quantal" peaks, which appeared by chance.

the quantal nature of neurotransmitter release (Dityatev et al., 1994; Kullmann, 1993; Larkman et al., 1992; Magleby and Miller, 1981; Rusakov, 1993; Stratford et al., 1997). These methods considered amplitude histograms as random processes, to which autocorrelation or spectral analyses could be applied to reveal the presence of periodic (sinusoidal) oscillations. Importantly, these methods do not require additional assumptions about specific mechanism of quantal release, i.e. they do not imply Poisson, binomial or compound binomial release processes (see Redman, 1990; Voronin, 1993b). Nevertheless, they have proved to provide estimates of the quantal size close to those provided by more constrained models (see Bart et al., 1988a; Bolshakov et al., 1997; Rusakov, 1993).

There is an obstacle to direct application of the standard spectral analysis to amplitude distributions. The latter represents a non-stationary process since quantal "oscillations" are superimposed with a monomodal "envelope", which can be considered as a low-frequency trend in terms of the time-series theory. To obtain unbiased estimates of periodic components from a short realization of the process, the trend should be subtracted. Early studies employed Gaussian curves as approximations to the experimental histograms (Bart et al., 1988a; Kullmann, 1993; Larkman et al., 1992). This can be considered satisfactory for many cases when experimental distributions are symmetrical and Gaussian-like. However, such a method could provide biased results when the actual experimental distributions are asymmetrical (see Bolshakov et al., 1997; Liao et al., 1992; Voronin et al., 1992a, 1992b, for examples of distributions). To correct for the non-stationarity we employed a polynomial approximation of cumulative amplitude distributions, as often used in time-series analysis (Dityatev et al., 1994). Coefficients of the polynomials were calculated by the least squares method (Press et al., 1986). We found that polynomials of eighth order provided a good fit to the cumulative functions derived from a variety of simulated and experimental data (Fig. 11A). The derivative of the theoretical cumulative function, i.e. of the fitted polynomial, provided a theoretical probability density function (PDF). An empirical PDF was calculated as a sum of Gaussian functions each having a measured amplitude value as its mean and a standard deviation equal to one-half S_n (Liao et al., 1992; see the chapter of Stricker and Redman, 2003 for optimal choice of the S.D.). The derivative of the polynomial (i.e. the "envelope" of the PDF) was subtracted from the experimental PDF (Fig. 11B), resulting in a curve fluctuating around zero and, thus, representing a stationary process (Fig. 11B, lower curve). The spectral density of this curve was computed using a fast Fourier transformation (Press et al., 1986). The reciprocal of the frequency having the maximum spectral density was taken as an estimate of Q (Fig. 11C). Having obtained an

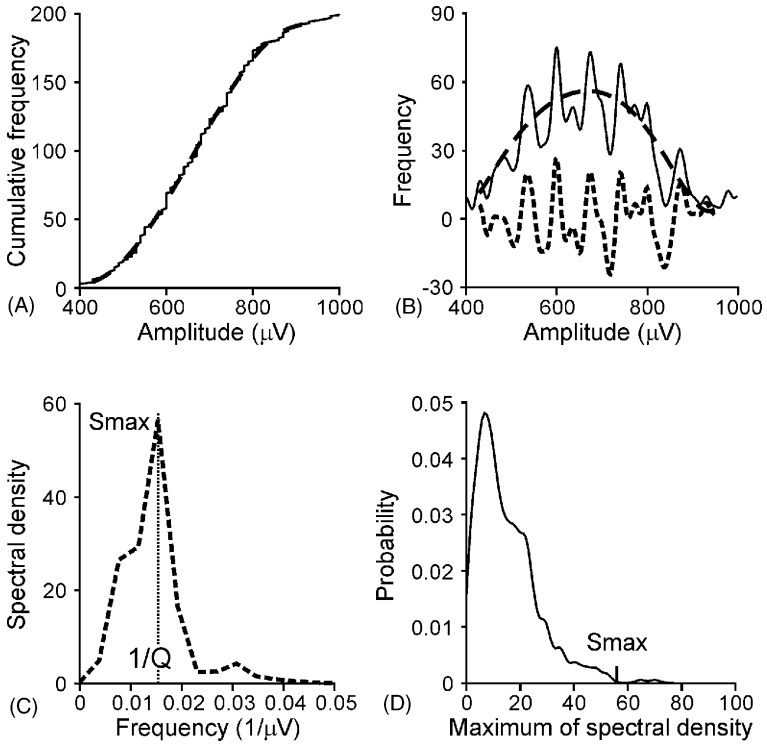

Fig. 11. Spectral analysis of sensorimotor EPSPs. (A) Experimental cumulative probability density function (steps) and its polynomial approximation (dashed curve). (B) Illustration of a filtering procedure. The lower bold dotted curve represents the difference between two upper curves that are experimental probability density function obtained by Gaussian kernel method (the upper curve having clearly visible peaks) and a derivative of the polynomial from A (dashed smooth curve). Frequency is the number of events multiplied by 100. (C) Spectral density of the lower curve from B. Maximum (S_{max}) corresponds to a quantal size (Q) of 67 μV. (D) Distribution of maxima of spectral densities for 1000 simulated data sets having a distribution described by the polynomial from A. S_{max} is the maximum value of the experimental spectral density. Modified from Dityatev et al. (1994).

estimate of Q by the spectral analysis, one can easily obtain an estimate for the mean quantal content m, as the ratio between mean amplitude of postsynaptic responses and Q.

The maximum value of the spectral density, S_{max}, was used to evaluate the significance of periodic oscillations by the Monte-Carlo method. For each experimental data set, we generated 100–1000 artificial data sets using the polynomial best fit to the experimental cumulative PDF. The PDFs of such simulated data sets resembled the PDF of the original data set but had no quantal peaks (Fig. 11B, upper dashed smooth curve). For each of the simulated data sets, the maximum of the spectral density was determined and compared with the maximum (S_{max}) calculated for the original data set (Fig. 11D). The fraction of data sets in which the maximum of the spectral density exceeded S_{max} was taken as the significance level (P) of the hypothesis that the original data set is derived from a continuous unimodal distribution. Experimental data sets with P less than a threshold value (0.05 or 0.1) were considered as having genuinely "peaky" distributions.

4.2. Application of spectral analysis to simulated and experimental data

To test the statistical properties of the estimates provided by the spectral analysis, data sets resembling experimental data but with known underlying distributions were generated. Afterwards, the values of Q and the significance (P) of apparent peaks were determined. A convolution of binomial and Gaussian distributions was used as an example of a "peaky" distribution, whereas Gaussian and chi-square distributions were used as "non-peaky" ones. We determined the effects of the sample size (N), number of quantal components (determined by binomial parameter n) and of their separation relative to S_n. As expected from results provided by other methods (Dityatev and Clamann, 1993), the spectral method overestimated Q values when the ratio Q/S_n was small. Surprisingly, the bias appeared to be independent of the number of the components in the underlying distribution ($n = 5$–20; Fig. 12A) and was not much larger for $N = 200$ as compared to $N = 500$ (Dityatev et al., 1994).

The power of the test to detect actual peaks was strongly dependent on the ratio between Q and S_n (Fig. 12B). The value of $Q/S_n = 2.5$ was critical: for lower values the test failed to reveal peaks, i.e. the probability of detection of a "peaky" distribution was not significantly different from the threshold P-value. It is important to note that the value 2.5 was critical for both $N = 500$ and 200. However, the values of the Q/S_n ratio that provided >50% successful detections of "peaky" distributions were different for different N: $Q/S_n = 3$ for $N = 500$ (Fig. 12B) and $Q/S_n = 3.5$ for $N = 200$.

In all previous computations, we searched for Q in a limited range from $0.8S_n$ to $4S_n$. We also checked that lifting these restrictions and selecting Q as the value corresponding to the global maximum of the spectral density did not reduce the power of the test to detect randomly generated peaks. However, this approach overestimated Q even at relatively high signal-to-noise ratios (Fig. 12A, upper curve), whereas the use of a restricted frequency domain produced proper estimates (Fig. 12A, lower curves).

To check that the method does not find significant peaks in the distributions where peaks do not exist, data samples from Gaussian distributions as well as chi-square distributions with 5 or 10 degrees of freedom were simulated. The probability of detection of "peaky" distributions is evidently dependent on the value of P, which defines how many such false detections we expect from the method. The number of false detections was found not to be significantly different

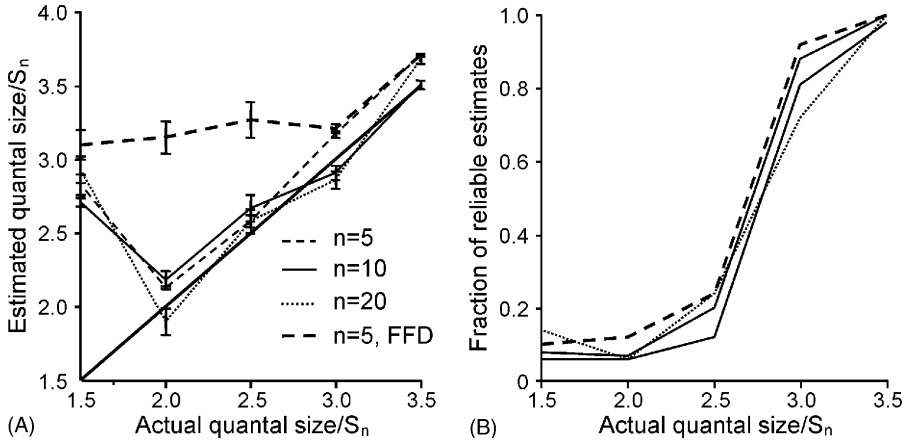

Fig. 12. Monte-Carlo analysis of reliability of quantal size estimated using the spectral analysis. (A) Dependence of the mean Q estimates on the noise standard deviation (S_n). Convolutions of binomial ($p = 0.6$; $n = 5$, 10 or 20) and Gaussian distributions ($Q/S_n = 1.5$, 2, 2.5, 3 or 3.5) were simulated with the sample sizes $N = 500$. The values of Q were adjusted to provide amplitude distributions with equal variances for different n. For each set of values of n, S_n and N, 100 data sets were generated. (A and B) Estimates obtained by restriction of frequency domain are indicated by dashed lines ($n = 5$), solid lines ($n = 10$) or heavy dotted line ($n = 20$). Heavy dashed lines correspond to estimates obtained using full frequency domain (FFD) for $n = 5$. (B) Dependence of the fraction of reliable Q estimates on the signal-to-noise ratio. For each data set from A, 100 new data sets were generated to calculate the fraction of reliable estimates. Modified from Dityatev et al. (1994).

from that expected. Therefore, the method satisfactorily rejected distributions with peaks that appeared by chance.

Since the Gaussian approximation was previously employed in a test for random peaks (Kullmann, 1993; Larkman et al., 1992), we compared the results of the subtraction of a polynomial with the subtraction of a Gaussian distribution. A chi-square distribution was used for these simulations. When the frequency range, in which the maximum of the spectral density was sought, was not restricted, the subtraction of a Gaussian distribution provided false detection of peaks in 90% of cases. In contrast, with subtraction of a polynomial, the probability of false detection was not significantly different from the threshold value ($P = 0.1$) even without restriction of the frequency domain.

Originally, a spectral analysis with polynomial subtraction was applied to 36 experimental data sets representing amplitude fluctuations of sensorimotor EPSPs recorded from the frog spinal cord (Dityatev et al., 1994). Among these, two amplitude distributions possessed peaks with a significance level $P = 0.005$. The estimates of Q obtained from these two distributions were 67 and 86 μV ($Q/S_n = 2.9$). For the rest of the data, $P > 0.1$ was found and the amplitude distributions were considered as "non-peaky". Thus, our analysis of the sensorimotor EPSPs in the frog spinal cord showed that only about 5% of the amplitude histograms had genuine peaks, whereas most of peaky experimental distributions might arise from sampling artifacts. Further analysis of 13 reticulospinal and 14 propriospinal EPSPs failed to reveal any peaky distributions, so that P was bigger than 0.1 in all these cases (Dityatev et al., 2001a, 2001b). Since the method proved by simulations to be rather powerful in detection of quantal distributions, these results suggest that there are factors, such as high number of spatially distributed synaptic contacts, which may mask quantal fluctuations in the frog spinal cord (see Section 6).

5. Method of moments

5.1. Estimation of quantal parameters

The selection of genuine quantal distributions is an important step to justify the use of several different approaches targeted to estimate parameters of quantal release (Dityatev and Clamann, 1993; Redman, 1990; Stricker et al., 1994; Voronin, 1993a). Some parameters could be estimated using so-called central moments of distributions. Here, for practical reasons, we consider just three moments, which define the mathematical expectation of the mean value (M_1), variance (M_2), and asymmetry (M_3) of a distribution. Their sample estimates are provided by the following simple expressions:

$$M_1 = \sum_{i=1}^{N} \frac{E_i}{N} \tag{1}$$

$$M_2 = \sum_{i=1}^{N} \frac{(E_i - M_1)^2}{N-1} \tag{2}$$

$$M_3 = \sum_{i=1}^{N} \frac{(E_i - M_1)^3}{N-2} \tag{3}$$

where E_i stands for the amplitude of a response with the sequential number i. In physiological literature, E and S^2 are often used instead of M_1 and M_2, respectively. In practice, the recorded signal is contaminated by a baseline noise, usually having Gaussian distribution with the first and third central moments equal to zero. To exclude the influence of the noise on the variability of response amplitudes, the variance of the background noise S_n^2 should be subtracted from the variance of recorded responses. Below we will refer to M_2 as the amplitude variance after subtraction of S_n^2.

In some cases, for instance, for the neuromuscular junction at low extracellular concentration of Ca^{2+}, numerous release sites are present with release probabilities close to zero. Then, the Poisson model can be used to describe amplitude fluctuations of postsynaptic responses. If the postsynaptic responses produced by a single quantum are of equal value Q, the first three moments of Poisson distribution are given by the following expressions:

$$M_1 = Qm \tag{4}$$

$$M_2 = Q^2 m \tag{5}$$

$$M_3 = Q^3 m \tag{6}$$

where m denotes the mean quantal content as defined in Section 1. The parameters Q and m could be derived from Eqs. (4) and (5) as

$$Q = \frac{M_2}{M_1} \tag{7}$$

$$m = \frac{M_1^2}{M_2} \tag{8}$$

The method of moments is based on the use of relationships between model parameters and moments of distributions. For the Poisson model, the estimates of the parameters are calculated from Eqs. (7) and (8) via substitution of the actual values of the moments M_i by their sample estimates. A very popular presentation of the last equation is

$$m = \mathrm{CV}^{-2} \tag{9}$$

where CV is the coefficient of variation of response amplitudes. It is defined as the ratio of the standard deviation of the response amplitude to its mean. This method of the estimate of the mean quantal content is often called "variance method" or "the method of the coefficient of variation" (see Faber and Korn, 1991; Voronin, 1993b for references).

One more popular method is calculation of m from the number of transmission failures (N_0). For the Poisson distribution

$$m = \ln\left(\frac{N}{N_0}\right) \tag{10}$$

Using this expression and Eq. (4), the quantal size is estimated as

$$Q = \frac{M_1}{\ln(N/N_0)} \tag{11}$$

In practice, however, the Poisson model usually cannot be applied to postsynaptic responses collected at normal extracellular Ca^{2+} concentration, when the release probabilities at different release sites (p_k) are rather far from 0. Also the assumption of a large number of release sites to be present in one connection is not valid for many central synapses. Then, if one can assume that p_ks are close to each other, the binomial model can be applied. In case of a uniform quantal size, the moments of the binomial model are given by the following expressions:

$$M_1 = Qnp \tag{12}$$

$$M_2 = Q^2np(1-p) \tag{13}$$

$$M_3 = Q^3np(1-p)(1-2p) \tag{14}$$

where Q, n and p stand for the quantal size, maximum number of quanta released (or the number of functional release sites) and probability of release, respectively. Using Eqs. (13) and (14), the binomial parameter p can be estimated as

$$p = \frac{M_2^2 - M_1M_3}{2M_2^2 - M_1M_3} \tag{15}$$

From Eqs. (12) and (13), binomial parameters $m = np$, n and p can be consecutively estimated using the following formula:

$$m = \frac{M_1(1-p)}{M_2} \tag{16}$$

$$Q = \frac{M_1}{m} \tag{17}$$

$$n = \frac{M_1}{Qp} \tag{18}$$

In practice, the estimate of p given by Eq. (15), however, was not in use. One possible reason is a high variability of M_3 for small data sets. Instead, researchers (Baskys et al., 1978; Dityatev et al., 1998, 2001a, 2001b; Voronin et al., 1992a) estimated binomial parameters using different combinations of M_1, M_2, N_0 and the maximum amplitude of postsynaptic responses (E_{max}). The latter is linked to the binomial parameters in the following manner (if S_n is negligible and N is large):

$$E_{max} = nQ \tag{19}$$

From Eqs. (19) and (12), p could be estimated as

$$p = \frac{M_1}{E_{max}} \tag{20}$$

Then, other parameters could be calculated using M_1 and M_2 from Eqs. (16)–(18) ("variance method"). It is obvious from Eq. (20) that with a small p (at limited N), E_{max} will be smaller than the theoretically predicted value, and therefore parameter p will be overestimated and n underestimated. When p is close to 1, addition of noise could lead to an underestimation of p. These predictions were confirmed by computer simulations (Voronin et al., 1992a). To improve determinations of the quantal parameters for small samples in the presence of background noise, a modified half-empirical formula was introduced for estimation of the binomial parameter p (Voronin, 1992a, 1993a, 1993b):

$$p = \frac{M_1}{E_{max3} - 0.3S_n \ln[2NM_1/(E_{max3} - S_n)]} \tag{21}$$

where E_{max3} stands for the mean value of three largest amplitudes. Computer simulations showed that this method reduced the bias of estimated binomial parameters and provided reasonably good estimates of binomial parameters in a broad range of n (1–15), p (0.05–0.95) and Q/S_n ratios (0.5–4) (Voronin et al., 1992a).

Similarly, m could be derived using N_0 and p provided by Eq. (20) or (21) ("failures method"):

$$m = \frac{p\ln(N_0/N)}{\ln(1-p)} \tag{22}$$

Then, n and Q are calculated using Eqs. (17) and (18).

Alternatively, p can be derived without the use of Eq. (20), but from Eqs. (16) and (22) as a numerical solution of the following equation ("combined variance-failures method", Voronin et al., 1992a):

$$\frac{(1-p)\ln(1-p)}{p} = \frac{M_2\ln(N_0/N)}{M_1^2} \tag{23}$$

Then, m, n and Q are calculated using Eqs. (16)–(18).

An essential limitation of the simple binomial model is the assumption that probabilities of release in different release sites are the same. There are numerous examples indicating that this assumption may be not valid for peripheral and central synapses. Importantly, this conclusion was made not only on the basis of statistical analysis of amplitude fluctuations (Bart et al., 1988a; Dityatev et al., 1992; Hessler et al., 1993; Walmsley et al., 1988), but also using independent methods of estimation of individual release probabilities in central synapses. These methods either employed a local stimulation of single boutons (Liu and Tsien, 1995) or utilized an open-channel blocker (MK-801) of glutamate receptors of NMDA type (Huang and Stevens, 1997; Rosenmund et al., 1993). If probabilities of release p_k at different release sites differ, the fluctuations of the postsynaptic responses are described by the compound binomial distribution (Walmsley et al., 1988) which has the following three moments:

$$M_1 = Q\sum_{k=1}^{n} p_k \tag{24}$$

$$M_2 = Q^2 \sum_{k=1}^{n} p_k(1 - p_k) \tag{25}$$

$$M_3 = Q^3 \sum_{k=1}^{n} p_k(1 - p_k)(1 - 2p_k) \tag{26}$$

In the general case when no additional assumptions about the distribution of p_k are made, the number of parameters in the compound binomial model is too high to use the method of moments. However, in a few particular cases, the method of moments can be applied. A simplest case is when two different classes of release sites co-exist, so that for all release sites of the first class the transmitter quanta are released with a probability equal to p_1, while all sites of the second class release neurotransmitter in response to every presynaptic spike ($p_2 = 1$). In this case, the release process is described by a convolution of two binomial distributions and the model parameters could be estimated from the following equations (Dityatev et al., 1992):

$$n_1 = \frac{4M_2^3}{M_2^2 - M_3^2} \tag{27}$$

$$p_1 = \frac{M_2 - M_3}{2M_2} \tag{28}$$

$$n_2 = M_1 - \frac{2M_2^2}{M_2 + M_3} \tag{29}$$

where n_1 and n_2 stand for the number of release sites of the first and second classes, respectively. This model has been applied for the analysis of sensorimotor EPSPs and showed better approximation of amplitude distributions than the simple binomial model (Bart et al., 1988b).

Another case of the compound binomial model is a beta-model that is based on the assumption that p_ks are distributed according to a beta-function. This function is used to describe p_k distributions because it is very flexible and can take a wide range of different shapes using two parameters a and b (Bennett and Lavidis, 1979; Clements and Silver, 2000; Zefirov and Stolov, 1982). The range includes monomodal distributions with a peak at 0, or at 1, or between 0 and 1, as well as bimodal distributions with peaks at 0 and 1. The formal definition of the beta distribution is

$$\text{probability}\,(p_k < x) = \frac{\int_0^x t^{a-1}(1-t)^{b-1}\,\mathrm{d}t}{\int_0^1 t^{a-1}(1-t)^{b-1}\,\mathrm{d}t} \tag{30}$$

Bennett and Lavidis (1979) and Zefirov and Stolov (1982) found that experimentally estimated distributions of p_ks at amphibian neuromuscular junctions could be well approximated by the beta-distributions and the beta-model can describe fluctuations of multiquantal responses. When n is sufficiently large, the moments of the beta-model are approximated by the following expressions:

$$M_1 = \frac{Qna}{a+b} \tag{31}$$

$$M_2 = \frac{Q^2 nab}{(a+b)(a+b+1)} \tag{32}$$

$$M_3 = \frac{Q^3 nab(b-a)}{(a+b)(a+b+1)(a+b+2)} \tag{33}$$

If parameter Q can be estimated, for instance, using the spectral analysis or analysis of miniature postsynaptic events (see the chapter of Bekkers, 2003), other parameters of a beta-distribution can be estimated by the method of moments as following:

$$n = \frac{2M_1(R_1 - R_2)}{R_1 + R_1R_2 - 2R_2} \tag{34}$$

$$a = \frac{R_1 + R_1R_2 - 2R_2}{1 + R_2 - 2R_1} \tag{35}$$

$$b = \frac{R_1 - R_1R_2}{1 + R_2 - 2R_1} \tag{36}$$

where $R_1 = M_2/(QM_1)$ and $R_2 = M_3/(QM_2)$.

5.2. Selection of a model using analysis of permissible values of moments

To decide which model of neurotransmitter release appropriately describes a given set of experimental data, the chi-square test is usually applied. This test compares frequencies of experimental histograms (H_j) and predicted theoretical values (F_j) using the following statistics:

$$\chi^2 = \sum_{j=1}^{L} \frac{(H_j - F_j)^2}{F_j} \tag{37}$$

where L is the number of binning classes in the amplitude histogram. This statistic has the chi-square distribution with the degree of freedom equal to $L - 1$ minus the number of independent model parameters. Therefore, it can be used to calculate the level of significance at which a particular model fits an experimental histogram.

Alternatively, one can analyze whether some indices derived from amplitude distributions have values specific for a particular model. The advantage of this approach is that indices calculated for many experimental data sets could be plotted together and compared to the regions of permissible values computed for several models (Fig. 13). This presentation provides a good overview of available data. To construct the most informative indices, it is important to exclude the influence of parameters present in all models related to quantal analysis, such as the mean quantal size Q and the number of release sites n. The influence of the latter can be excluded by considering ratios between moments. If Q can be estimated by an independent method, one can use the following indices:

$$R_1 = \frac{M_2}{M_1 Q}, \qquad R_2 = \frac{M_3}{M_2 Q} \tag{38}$$

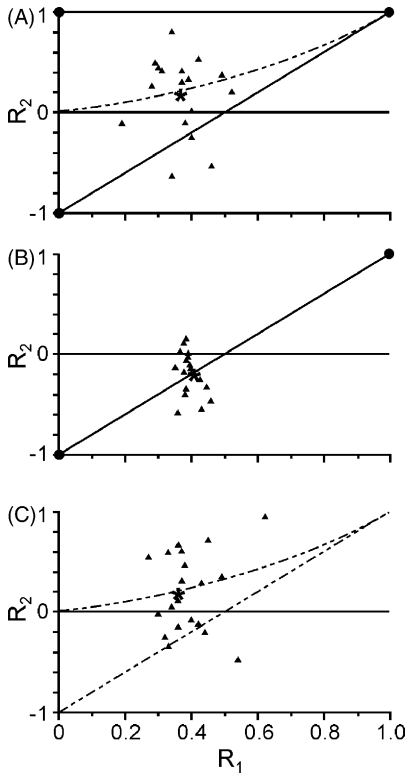

Fig. 13. Analysis of permissible values of moments. (A) Scatter plots of R_1 and R_2 values calculated for 17 samples of frog sensorimotor EPSPs. R_1 and R_2 were calculated from Eq. (38). Permissible values of R_1 and R_2 for the binomial model (A and B) are located along the line connecting large dots at (0, −1) and (1, 1). The triangle marked by the large dots and a region outlined by dashed lines correspond to the region of permissible values for convolution of two binomial distributions (A) and the beta-model (A and C), respectively. (B and C) Similar plot as in A, but for 20 data sets simulated assuming the binomial (B) or beta-model of quantal release (C). The center of experimental (A) or simulated values (B and C) is marked by (∗). The following parameters were used for the simulations: $n = 15$, $p = 0.6$ (B); $n = 45$, $a = 0.17$, $b = 0.68$ (C). Sample size was 400 in all simulations. Modified from Dityatev et al. (1992).

These indices do not depend on Q and n, although their values are functions of other parameters influencing fluctuations of postsynaptic responses, such as the mean probability of release and variance of p_k. Evidently, these indices have meanings similar to the coefficient of variation and the coefficient of asymmetry. Their values for the Poisson model are equal to 1, as could be easily derived from Eqs. (4)–(6). For the binomial model, Eqs. (12)–(14) show that the R_1 and R_2 are linked by the following relation:

$$R_2 = 2R_1 - 1 \tag{39}$$

Thus, all possible theoretical R_1, R_2 values for the binomial model would lie along a diagonal line connecting points with coordinates (0, −1) and (1, 1) (Fig. 13A and B). Our analysis of Eqs. (24)–(26) (Dityatev et al., 1992) revealed that all possible theoretical values of R_1 and R_2 for a convolution of two binomial distributions lay within a triangle marked by the large dots in Fig. 13A. For the beta-model, theoretical values of R_1 and R_2 lay within a region limited by the dashed lines shown in Fig. 13A and C. The lower border of R_1, R_2 regions for the convolution of two binomial distributions as well as for the beta-model corresponds to the binomial model. The upper dashed line is defined by the following expression:

$$R_2 = \frac{R_1}{1 - R_1} \tag{40}$$

Moments and regions of permissible values for several other models of transmitter release have been reviewed by Dityatev et al. (1992).

The expressions described above are evidently valid for infinitely large samples. To analyze variability of R_1, R_2 values for finite samples, we generated data sets for several models using the Monte-Carlo method. We found that R_1 and R_2 obtained for the simulated sets form clusters around the actual values used for simulations (Fig. 13B and C). For instance, for the binomial model, simulated values of R_1 and R_2 were near the line corresponding to the binomial model (Fig. 13B). For the beta-model, the values of R_1 and R_2 for the simulated data sets lay within or nearby the region of permissible values for the beta-model, as shown in Fig. 13C. There was a higher variability of the simulated R_1 and R_2 values for the beta-model, as compared to the binomial model (Fig. 13B and C), although the same $N = 400$ was used for simulations.

For the sensorimotor EPSPs recorded from the spinal cord of the frog (Dityatev et al., 1992), most of calculated R_1 and R_2 values were found to lie above the line corresponding to the binomial model (Fig. 13A). As was found in our simulations (Fig. 13B), approximately half of points should lie below the bisector if the binomial model underlay neurotransmitter release in this connection. This discrepancy was significant ($P < 0.01$, chi-square test). Importantly, experimental values of R_1 and R_2 form a cluster with the center located within the region of permissible values for the beta-model. Furthermore, the scatter patterns of the experimental points (Fig. 13A) and data simulated with the use of beta-model (Fig. 13C) showed remarkable similarity, supporting a view that the beta-model adequately describes transmitter release in the sensorimotor connections of the frog spinal cord.

6. Discussion

6.1. Principal component analysis

We showed applicability of the PCA to minimal hippocampal (present data) and neocortical (Akaneya et al., 2003) responses. One peculiarity of this application in comparison with most of previous electrophysiological studies (Barth and Di, 1992; Chapman and McCrary, 1995; Glaser and Ruchkin, 1976, but see Musial et al., 1998) is using single (non-averaged) responses as the input data. Therefore, the results can be useful for further analysis of single trials including building of amplitude distributions (Fig. 1G) and

quantal analysis. The standard PCA gives C1 scores, which can be used instead of conventional amplitude or slope measurements. Such "PCA amplitudes" (Fig. 1E) utilize more information about the waveform as compared to the conventional measures (Chapman and McCrary, 1995).

As noted by the authors who recorded electrical evoked potentials (e.g. Collet, 1989), the physiological meaning of the PCA components might be uncertain. To facilitate their interpretation, we elaborated procedures for extraction of distinct waveforms. We showed that hippocampal minimal EPSPs often can be separated into two (sometimes three) distinct components with different latencies and/or time courses. The simplest interpretation of this result is that more than one presynaptic fibre or release site is activated by minimal stimulation (see Section 1). Indeed, even a single axon branch can contact two to four different dendrites of a target CA1 neuron (Harris and Kater, 1994) so that the related synapses can be spatially remote and produce postsynaptic responses with different latencies and kinetics. Moreover, in addition to the monosynaptic inputs, such as the Schaffer collaterals or local circuit connections to CA1 neurons (Thomson and Deuchars, 1995), polysynaptic pathways can be activated. Our analysis showed approximately similar latency variations for the early and late components in most cases, suggesting that both detected components were monosynaptic. The signs of polysynaptic activation, namely, longer latency and stronger variations as compared to the EPSP components that we detected with the measurement window covering initial EPSP slope, were much less common. Therefore, we believe that significant polysynaptic activation was unlikely under our conditions (minimal stimulation, cut between CA3 and CA1).

The interpretation of the EPSP components based on activation of different synaptic sites is strongly supported by the simulation experiments with the number and shape of the components known. The plots of the component scores in the simulation experiments appeared to be strikingly similar to those in our physiological experiments. Several additional observations are compatible with physiological meaningfulness of the EPSP components. (1) When different components were suspected from considerations of single or average responses (Fig. 4A and B), the PCA-based component analysis produced the expected number of components. (2) Comparison of EPSP1 and EPSP2 gave expected results: the same respective components, characteristic PPF, parallel post-tetanic changes, smaller post-tetanic increases for EPSP2 as compared to EPSP1 scores. The latter observation agrees with post-tetanic decreases in the PPF ratio typically observed under our conditions (Sokolov et al., 1998; see also Kleschevnikov et al., 1997; Kuhnt and Voronin, 1994) and by others (Li et al., 2000; Schulz, 1997). (3) Dissimilar changes of different components in the course of our experiments (Fig. 6D and E) confirm that they represented independent identities. (4) PCA of the background noise produced scores of about zero with occasionally large values, which typically corresponded to spontaneous events similar to EPSPs by their waveforms. (5) Responses with scores of about zero usually represented transmission failures (Fig. 4F4). (6) Combined component and pharmacological analyses produced expected extraction of components mediated by the two different subtypes of glutamate receptors (Fig. 9).

The existence and heterogeneous behaviour of components with different latencies and time courses have several implications. As an example, we shall briefly discuss their relation to several phases of LTP maintenance in CA1 synapses (Bliss and Collingridge, 1993). Our recording period corresponded to two phases: LTP1 (termed also STP by some authors) which covers the initial 15–60 min according to different publications, and LTP2, which develops slower and lasts up to 3–4 h. There is no general agreement on LTP1 and LTP2 mechanisms. For example, LTP1 was explained by primarily presynaptic (Bliss and Collingridge, 1993; Kullmann et al., 1996; Voronin, 1993a, 1993b) or postsynaptic (Edwards, 1995; Malenka and Nicoll, 1999) modifications. The present data suggest a new view, according to which different synaptic sites (or even inputs) may be responsible for different phases. The delayed (15–60 min) potentiation of one of the components suggests that LTP2 may be due to morphological changes. Appearance of synapses with completely separated transmission zones (Geinisman et al., 1993) represents a plausible possibility (see also Edwards, 1995; Kleschevnikov et al., 2002; Sokolov et al., 2002; Voronin et al., 1995).

Thus, we demonstrated that PCA is applicable to minimal postsynaptic responses. We described procedures which separate physiologically meaningful EPSP components presumably arising from activation of different fibres or release sites. Under realistic signal-to-noise ratios (>2–3) the algorithm resolves EPSP components with differences in latency of 0.8–1 ms or in T_{rise} of 2–3 ms. In practice, the sensitivity is often even higher (0.6 and 1.6 ms, respectively) because differences in both latency and T_{rise} are very common. From the methodological point of view, the PCA application can be considered as a way to substitute recordings of single-fibre EPSPs for a less laborious and more stable recordings of minimal postsynaptic responses. Recently we used this approach in practice to separate activation of mossy fibre and associative/commissural fibre inputs to CA3 pyramidal neurons (Berretta et al., 2000) and two inputs to neurons of visual cortex activated by minimal intracortical stimulation (Akaneya et al., 2003). In addition, the component analysis can be used for more precise analysis of unitary postsynaptic responses separating activation of different transmission zones and even of different receptor types of the same transmission zone.

Summarizing this part, we conclude that the PCA-based algorithm has at least two advantages important for quantal analysis. The first one is a less noisy measure of the response magnitude, as compared to the common peak amplitude, independent of whether only one or more components are present. The second is the possibility of separate calculation of quantal parameters for different components,

which in turn could help to avoid false results that could appear when mixed responses which consisted of several components are analyzed.

6.2. Spectral analysis

Several methods of time-series analysis have been used to evaluate significance of apparent equally spaced peaks in amplitude distributions (Dityatev et al., 1994; Kullmann, 1993; Larkman et al., 1992; Magleby and Miller, 1981; Rusakov, 1993). The approach presented in this review is distinguished by (1) the subtraction of polynomial "envelop" from amplitude distributions; (2) the use of fast Fourier transformation to compute spectra; and (3) the use of Monte-Carlo simulations to evaluate the significance of periodic peaks (P).

It seems to be important to use the polynomial approach for the following reason: When the envelope of a histogram is not exactly Gaussian (or another function with a fixed shape), the residual trend after the subtraction of the Gaussian curve from an amplitude distribution makes a significant contribution to the spectral density, particularly at low frequencies, and consequently to the maximum of the spectrum, S_{max}. As a result, the maxima of the spectral densities of the simulated Gaussian distributions used in calculations of P are systematically smaller than S_{max}, even when the analyzed distribution had no peaks. Therefore, the number of distributions with significant peaks is overestimated. Employing the maximum entropy method to calculate spectral density (Kullmann, 1993) seems to avoid this problem if only a few coefficients of the autocorrelation are used. However, the part of the spectral density that is subtracted in this way and how many coefficients should be optimally used have not yet been determined.

To determine the significance of the periodic oscillations, theoretically the variance analysis (commonly known as ANOVA) can be used: If there are no systematic oscillations and, thus, the analyzed process represents a set of independent observations, spectral amplitudes should be distributed according to a chi-square distribution with two degrees of freedom. This approach has been applied to a few examples of experimental and simulated data (Rusakov, 1993), but statistical evaluation for the bias and reliability of provided estimates remains to be performed. An obvious limitation is that this method has to be applied to amplitude histograms (Rusakov, 1993) and therefore depends on the binning of the primary data. Moreover, the presence of a trend or even its residuals left after the trend subtraction could lead to an overestimation of the spectral amplitudes of the oscillations and, therefore, to false detection of oscillations. To avoid the above-mentioned biases and evaluate the significance of periodic oscillations, the use of Monte-Carlo simulations therefore seems to be advantageous.

Our simulations showed that to obtain unbiased results, the required value of the Q/S_n ratio must be more than 2.5. For S_n of 30–40 μV this requires Q equal to at least 75–100 μV. The fact that only a few estimates of quantal size in frog synapses were found to be reliable means that these synapses rarely express quantal sizes as large as these values. An additional source of "noise" occurs if there is a significant quantal variability in these synapses. In this case, the variance of the apparent noise for a given peak in the amplitude histogram would be equal to the sum of S_n^2 plus the intrinsic variance of the quantal size multiplied by a constant equal to the sequential number of the peak (Baskys et al., 1979; Voronin, 1993b; but see Jack et al., 1994). For the spinal cord EPSPs, the latter term can be high due to the fact that many boutons mediate synaptic transmission in the connection established by a single muscle afferent fibre or descending axon. Additionally, spatial non-uniformity of Q across different release sites, for instance, due to variability of their locations, can contribute to the variability of the quantal size. Thus, the complexity of the spinal cord synapses may account for the fact that the number of distributions with significant multiple quantal peaks obtained for these synapses was lower than the 53% (8 of 15) and the 19% (8 of 42) derived for potentiated and non-potentiated hippocampal synapses of the rat by our method (Bolshakov et al., 1997) or by a similar technique (Kullmann, 1993).

6.3. Method of moments

When correctly applied, the method of moments provides unbiased and robust estimates of the basic quantal parameters. This method is simple and has been widely used in numerous in vitro studies, especially in initial studies on neuromuscular junctions under conditions when transmitter release was artificially suppressed by lowering the ratio of Ca^{2+} to Mg^{2+} concentrations in the external medium (see reviews listed in Section 1 for references). In the central synapses, the estimates of quantal parameters derived from the number of transmission failures as well as from the value of CV^{-2} have also been used in numerous publications, for example, to evaluate contribution of presynaptic mechanisms in synaptic plasticity (for references, see e.g. Faber and Korn, 1991; Voronin, 1993a). Limitations of the application of the coefficient of variation method to the Poisson and to the more general binomial model have been considered by Faber and Korn (1991).

When applied to CA1 hippocampal synapses, the above methods based on a binomial distribution (Eqs. (16)–(23)) all gave consistent results (Voronin et al., 1992a) that were close to those provided by deconvolution analysis based on a quantal model not constrained by the binomial law (Voronin et al., 1992b). In the spinal cord, the estimates of the binomial parameter p obtained from Eq. (20) showed a strong negative correlation with the magnitude of subsequent post-tetanic potentiation (Dityatev and Clamann, 1998), as is expected when synapses with a high efficacy of transmitter release would be close to saturation, whereas synapses with low p could be further potentiated. Unitary EPSPs evoked in two different motoneurons of the lumbar spinal cord by stimula-

tion of the same descending axon showed considerable differences in the mean amplitudes. These differences appeared to be related to the distance between postsynaptic motoneurons and were mostly expressed in terms of binomial parameters n and p, rather then Q (Dityatev and Clamann, 1998).

In the sensorimotor connections of the frog, analysis of permissible values of moments suggests the spatial non-uniformity of transmitter release probabilities, which could be described by the beta-model. Additional support for the beta-model is obtained by comparison of the numbers of boutons contacting a motoneuron (derived from morphological reconstructions) and estimated values of parameter n (Dityatev et al., 1992). There is a striking one-to-one relationship between these values ($r = 0.95$, five connections). Respective beta-model parameters ($a = 0.17$ and $b = 0.68$) indicate extremely high non-uniformity of release probabilities: a beta-function with these parameters has two maxima, the most prominent one at 0 (low-efficient release sites) and the second maximum at 1 (highly efficient release sites). Thus, these data correspond to results previously obtained using the convolution of two binomial distributions (Bart et al., 1988b), which also predicted existence of highly efficient release sites in sensorimotor connections. It would be of great interest to plot the R_1 and R_2 values for other types of synapses and relate these to regions of permissible values for several known models of transmsitter release.

7. Conclusions

In summary, the data of this chapter demonstrate that "early" steps in evaluation of experimental data are very important for subsequent quantal analysis. The best possible signal-to-noise ratio should be achieved. We show that the methods based on the principal component analysis allow one to optimally measure unitary and minimal postsynaptic responses. This approach gives selective measurements of different separate components that can be present in both unitary and especially minimal postsynaptic responses making subsequent quantal analysis more precise and allows one to avoid possible false results. Further, we show that spectral analysis is a method of choice to determine whether peaks in the distributions of amplitudes of postsynaptic responses are regular and genuine or appeared by chance. Finally, we demonstrate how the method of moments could be used to estimate parameters of several models and argue that a plot of moment ratios (R_1 and R_2) graphically depicts variability and asymmetry of multiple experimental distributions. This provides a convenient way to test or at least to formulate plausible hypotheses on the mechanisms of transmitter release.

Acknowledgements

We thank all members of our and collaborating groups for their collaboration and useful discussions. Special thanks are to Drs. I. Bayazitov, E. Cherubini, S. Gasparini, V.I. Derevyagin, A.M. Kleschevnikov, A.V. Rossokhin, M.V. Sokolov, L.P. Savtchenko, S. Gapanovich, V. Kozhanov, A. Babalyan, N. Chmykhova, and H.P. Clamann for participation in parts of this work. We thank C. Patton and M. Hammond for improving the English and especially Dr. D.S. Faber for critical reading of the manuscript and numerous suggestions. This work was supported by grants from INTAS, RFBR and from Wellcome Trust to L.L.V. and from DFG to A.E.D.

Appendix A. Principal component analysis and its application to minimal postsynaptic responses

A.1. Basic formula of the principal component analysis

As briefly described in the text of this review, the principal component analysis is a method of the multivariate statistics that finds the most important directions of the data variance in a linear fashion. Here we give the standard formal introduction of PCA (Harmon, 1979; Jackson, 1991) and describe a PCA algorithm adapted for analysis of minimal and unitary postsynaptic potentials responses recorded intracellularly in electrophysiological experiments. The application of the algorithm to the physiological and simulated waveforms is described in the main text.

Let $S_i(t)$ be a function describing the waveform of a single postsynaptic PSP or PSC with number i ($i = 1, 2, \ldots, N$) from a set of N responses. Let $S_i(t)$ be defined by a set of consecutive numbers S_{it}, i.e. we take amplitude measurements from a window of T discrete time points. It is convenient to align the measurements in such a way that the mean amplitude of each single response over the window was equal to 0. The basic assumption of PCA is that the set of the data waveforms S_{it} can be represented as a linear combination of K independent fundamental waveforms (components) f_{kt}. In our case, PSP/PSC waveform S_{it} recorded in time bin t on trial i can be represented as a linear combination of responses from K independent inputs plus noise (B_{it}). Therefore

$$S_{it} = \sum(k = 1 \text{ to } K) c_{ik} f_{kt} + B_{it} \tag{A.1}$$

where the weighting coefficients or scores c_{ik} indicate the weight of each component present on each trial. Each component (f_{kt}) represents a temporal pattern of the fundamental waveforms underlying variability of postsynaptic responses. If we ignore the noise, the following procedure may be used to find the first component (C1) or f_{1t}. We assume

$$\sum(t = 1 \text{ to } T) f_{1t}^2 = 1 \tag{A.2}$$

and define C1 scores as

$$c_{i1} = \sum(t = 1 \text{ to } T) f_{1t} S_{it} \tag{A.3}$$

Let the "residual" $S(1)_{it} = (S_{it} - c_{i1} f_{1t})$. From Eqs. (A.2) and (A.3) it follows: $\sum f_{1t} S(1)_{it} = 0$. Therefore we find f_{1t}

so that the sum of respective residuals for all N responses is minimal, i.e. $\sum(i = 1 \text{ to } N) \sum(t = 1 \text{ to } T)(S(1)_{it})^2 \rightarrow \min$, which is equivalent to

$$\sum(i = 1 \text{ to } N)c_{i1}^2 \rightarrow \max \quad \text{(A.4)}$$

After finding f_{1t}, we calculate the second component (f_{2t}) or C2 using equations similar to Eqs. (A.2) and (A.3), i.e. $\sum f_{2t}^2 = 1$, $c_{i2} = \sum(t = 1 \text{ to } T) f_{2t} S(1)_{it}$, the condition of components "orthogonality" in the space of response amplitudes ($\sum f_{1t} f_{2t} = 0$), and a minimization procedure $\sum(i = 1 \text{ to } N) \sum(t = 1 \text{ to } T)(S(2)_{it})^2 \rightarrow \min$. Here, the residual $S(2)_{it} = S_{it} - c_{i1} f_{1t} - c_{i2} f_{2t}$. Again similar to Eq. (A.4), $\sum c_{i2}^2$ is maximized. The procedure can be repeated until the Kth component is determined. As a result, each response is described in new coordinates (c_{i1}, c_{i2}, ..., c_{iK}) instead of the previous temporal coordinates S_{it}.

A.2. "Optimization" of the number of principal components

The importance of PCA is its ability to adequately represent a T variable data set in $K < T$ dimensions. The larger K, the better is the fit of the PCA model to experimental data. The smaller K, the simpler the model. Determination of the optimal value of K ("when to stop?", see Jackson, 1991) is essential: it permits one to ignore components that explain very little of the total variance and, in addition, may not be readily interpretable. There are a large number of criteria (Jackson, 1991), but generally the problem of K determination does not seem to be solved.

In our case, the components, which describe noise, do not represent any essential interest. Therefore, to optimize K, we compared PCA results obtained from the responses and from the background noise. The idea was formulated as follows. For every k from Eq. (A.1), let define the squared mean deviation of the PCA scores from 0: $w_k = (1/N) \sum(i = 1 \text{ to } N)(c_{ik})^2$. Let B_{it} represent the background noise, in the same way as S_{it} (see Eq. (A.1)). Then, we can define scores h_{ik} in the PCA basis: $h_{ik} = \sum(t = 1 \text{ to } T) B_{it} f_{kt}$ and calculate $d_k = (1/N) \sum(i = 1 \text{ to } N) h_{ik}^2$. If a component does not contain any information about the response, i.e. it corresponds to the noise, w_k should be approximately equal d_k, where $k = 1, 2, \ldots, K$ is the number of the components. Therefore, we considered the sequence $o_k = w_k/d_k$ which was decreasing and tended to approach 1. According to our criteria we can ignore components which give o_k smaller than a certain constant (e.g. 1.2). As exemplified in the main text (Fig. 3C), the two-dimensional plots of the last simulated component against the next (non-simulated) component represented a band with its width comparable to that of the respective plot for the noise, i.e. passing the above criterion. In practice, on the basis of the analysis of physiological data we used $K = 5$.

A.3. Alignment procedure and identification of response components

For identification of the components, an alignment procedure was elaborated and tested in simulation experiments and against physiological data as described in the main text. If K is the "optimal" number of components as defined in the previous section, we can consider the following signal representation instead of Eq. (A.1): $S_{it} = \sum(k = 1 \text{ to } K) c_{ik} f_{kt} + R_{it}$, where R_{it} is a small residual which we can ignore. To facilitate physiological interpretation of the components we can define new functions F_{lt} so that $S_{it} = \sum(l = 1 \text{ to } K) C_{il} F_{lt}$. We shall look for F_{lt} in the form: $F_{lt} = \sum(k = 1 \text{ to } K)\ A_{lk} f_{kt}$. Therefore, $f_{kt} = \sum(l = 1 \text{ to } K) A'_{lk} F_{lt}$, where the matrix A' is the inverted matrix A. Then $C_{il} = \sum(k = 1 \text{ to } K) c_{ik} A'_{lk}$, i.e. the coefficients C_{il} can be obtained from c_{ik} in Eq. (A.1) by a linear transformation. To facilitate component identification we performed a transformation of the two-dimensional plots according to the following four conditions. First, the dots around (0, 0) coordinate should preserve their position within $\pm 2S_n$ (where S_n is the noise standard deviation for the respective component). This condition follows from the above formulations of the linear transformation of the coefficients c_{ik} into C_{il}. Second, all C_{il} should be positive within $\pm 2S_n$. This condition is natural for purely excitatory inputs. Third, the borders of the component plots should be aligned along the coordinate axes (see Fig. 3Da and b of the main text). The objective was to obtain a full range of "pure" component scores for one input (response component), which corresponds to about zero values for the other input. This condition stresses one limitation of our identification procedure: the presence of response failures for every component to be unequivocally identified. Fourth, if the plot contains gaps (see Fig. 3Db of the main text) they should also be aligned. This condition is natural because the gaps reflect "quantization" which creates additional borders. The borders facilitated the alignment, especially when the sample size and N_0 were low.

References

Akaneya Y, Altinbaev RSh, Bayazitov IT, Kinoshita S, Voronin LL, Tsumoto T. Low-frequency depression of synaptic responses recorded from rat visual cortex. Neuroscience 2003;117:305–20.

Alger BE, Pitler TA, Wagner JJ, Martin LA, Morishita W, Kirov SA, Lenz RA. Retrograde signalling in depolarization-induced suppression of inhibition in rat hippocampal CA1 cells. J Physiol London 1996;96:197–209.

Astrelin AV, Sokolov MV, Behnisch T, Reymann KG, Voronin LL. Noise deconvolution based on the L1-metric and decomposition of discrete distributions of postsynaptic responses. J Neurosci Methods 1997;3:17–27.

Astrelin AV, Sokolov MV, Behnisch T, Reymann KG, Voronin LL. Principal components analysis of minimal excitatory postsynaptic potentials. J Neurosci Methods 1998;79:169–86.

Auger C, Marty A. Quantal currents at single-site central synapses. J Physiol London 2000;526:45–53.

Babalian AL, Chmykhova NM. Morphophysiological characteristics of connexions between single ventrolateral tract fibres and individual motoneurones in the frog spinal cord. Brain Res 1987;407:394–7.

Barrett EF, Stevens CF. The kinetics of transmitter release at the frog neuromuscular junction. J Physiol London 1972;227:691–708.

Bart AG, Dityatev AE, Kozhanov VM. Quantal analysis of the postsynaptic potentials in the interneuronal synapses: Recovery of a signal from the noise. Neurophysiology/Neirofiziologiia 1988a;20:479–87.

Bart AG, Ditiatev AE, Kozhanov VM. An analysis of transmission in the interneuronal synapses using a convolution of binomial distributions. Neurophysiology/Neirofiziologiia 1988b;20:487–94.

Barth DS, Di S. Topographical analysis of epileptiform potentials in rat somatosensory cortex: the interictal to ictal transition. Brain Res 1992;91:33–43.

Baskys A, Voronin LL, Derevyagin VI. Analysis of mechanisms of frequency potentiation of synaptic responses in hippocampal neurons. Doklady Biol Sci 1978;239:234–7.

Baskys A, Voronin LL, Gusev LN, Derevyagin VI, Kesarev VS, Logunov DB, Shidarev DR. Calculations of theoretical amplitude distributions of postsynaptic potentials for quantal analysis. Neurophysiology/Neirofiziologiia 1979;20:146–50.

Bayazitov IT, Voronin LL, Kasyanov AM, Kleschevnikov AM, Kulchitsky SV, Sametsky E. Long-term potentiation of the AMPA and NMDA components of minimal postsynaptic currents in rat hippocampal field CA1. Neurosci Behav Physiol 2002;32:533–40.

Bekkers JM, Stevens CF. Application of quantal analysis to the study of long-term potentiation: errors, assumptions, and precautions. In: Baudry M, Davis J, editors. Long-term potentiation: a debate of current issue. Cambridge, MA: MIT Press; 1991. p. 64–76.

Benke TA, Luthi A, Isaac JT, Collingridge GL. Modulation of AMPA receptor unitary conductance by synaptic activity. Nature 1998;393:793–7.

Bennett MR, Lavidis NA. The effect of calcium ions on the secretion of quanta evoked by an impulse at nerve terminal release sites. J Gen Physiol 1979;74:429–56.

Berretta N, Rossokhin AV, Cherubini E, Astrelin AV, Voronin LL. Long-term synaptic changes induced by intracellular tetanization of CA3 pyramidal neurons in hippocampal slices from juvenile rat. Neuroscience 1999;93:469–77.

Berretta N, Rossokhin AV, Kasyanov AM, Sokolov MV, Cherubini E, Voronin LL. Postsynaptic hyperpolarization increases the strength of AMPA mediated synaptic transmission at large synapses between mossy fibres and CA3 pyramidal cells. Neuropharmacology 2000;39:2288–301.

Blanton MG, Lo Turkco JJ, Kriegstein AR. Whole cell recording from neurons in slices of reptilian and mammalian cerebral cortex. J Neurosci Methods 1989;30:203–10.

Bliss TVP, Collingridge GL. A synaptic model for memory: long-term potentiation in the hippocampus. Nature 1993;361:31–9.

Bolshakov VY, Golan H, Kandel ER, Siegelbaum SA. Recruitment of new sites of synaptic transmission during the cAMP-dependent late phase of LTP at CA3–CA1 synapses in the hippocampus. Neuron 1997;19:635–51.

Chapman RM, McCrary JW. EP component identification and measurements by principal components analysis. Brain Cognition 1995;27:288–310.

Churchland PS, Sejnowski TJ. The computational brain. Cambridge, MA: MIT Press; 1992.

Clements JD, Silver RA. Unvelling synaptic olasticity: a new graphical and analytical approach. Trends Neurosci 2000;23:105–13.

Collet W. Doubts on the adequacy of the principal component varimax analysis for the identification of event-related brain potential components: a commentary on Glaser and Ruchkin. Biol Psychol 1989;28:163–72.

Debanne D, Guerineau NC, Gahwiler BH, Thompson SM. Paired-pulse facilitation and depression at unitary synapses in rat hippocampus: quantal fluctuation affects subsequent release. J Physiol London 1996;491:163–76.

Del Castillo J, Katz B. Quantal component of the end plate potential. J Physiol London 1954a;124:560–73.

Del Castillo J, Katz B. Statistical factors involved in neuromuscular facilitation and depression. J Physiol London 1954b;124:574–85.

Dityatev AE, Clamann HP. Limits of quantal analysis reliability: quantal and unimodal constraints and setting of confidence interval for quantal size. J Neurosci Methods 1993;50:67–82.

Dityatev AE, Clamann HP. Synaptic differentiation of single descending fibers studied by triple intracellular recording in the frog spinal cord. J Neurophysiol 1998;79:763–8.

Dityatev AE, Kozhanov VM, Gapanovich SO. Modeling of the quantal release at interneuronal synapses: analysis of permissible values of model moments. J Neurosci Methods 1992;43:201–14.

Dityatev AE, Kozhanov VM, Gapanovich SO, Clamann HP. Quantal analysis based on spectral methods. Pflugers Arch 1994;429:22–6.

Dityatev AE, Birinyi A, Puskár Z, Antal M, Clamann HP. Monosynaptically connected long propriospinal axon—motoneuron pairs in the lumbar spinal cord of frogs. A correlative physiological and morphological study. Neuroscience 2001a;106:405–17.

Dityatev AE, Chmykhova NM, Dityateva GV, Babalian AL, Kleinle J, Clamann HP. Structural and physiological properties of synapses formed by individual reticulospinal fibers on lumbar motoneurons of the frog. J Comp Neurol 2001b;430:433–47.

Durand GM, Kovalchuk Y, Konnerth A. Long-term potentiation and functional synapse induction in developing hippocampus. Nature 1996;381:71–5.

Edwards FA. LTP—a structural model to explain the inconsistencies. Trends Neurosci 1995;18:250–5.

Edwards FA, Konnerth A, Sakmann B, Takahashi T. A thin slice preparation for patch clamp recordings from neurons of the mammalian central nervous system. Pflugers Arch 1989;414:600–12.

Edwards FA, Konnerth A, Sakmann B. Quantal analysis of inhibitory synaptic transmission in the dentate gyrus of rat hippocampal slices: a patch clamp study. J Physiol London 1990;430:213–49.

Faber DS, Korn H. Application of the coefficient of variation methods for analyzing synaptic plasticity. Biophys J 1991;60:1288–94.

Feldmeyer D, Sakmann B. Synaptic efficacy and reliability of excitatory connections between the principal neurones of the input (layer 4) and output layer (layer 5) of the neocortex. J Physiol London 2000;525:31–9.

Foster TC, McNaughton BL. Long-term enhancement of CA1 synaptic transmission is due to increased quantal size, not quantal content. Hippocampus 1991;1:79–91.

Friston KJ. Computational approaches to quantifying human neuroanatomical variability. In: Toga AW, Mazziotta JC, editors. Brain mapping. San Diego: Academic Press; 1996. p. 363–85.

Gasparini S, Saviane C, Voronin LL, Cherubini E. Silent synapses in the developing hippocampus: lack of functional AMPA receptors or low probability of glutamate release? Proc Natl Acad Sci USA 2000;97:9741–6.

Geinisman Y, de Toledo-Morell L, Morell F, Heller RE, Rossi M, Parshall RF. Structural synaptic correlate of long-term potentiation: formation of axospinous synapses with multiple, completely partitioned transmission zones. Hippocampus 1993;3:435–46.

Glaser EM, Ruchkin DS. Principles of neurobiological signal analysis. New York: Academic Press; 1976.

Grantyn R, Shapovalov AI, Shiriaev BI. Relation between structural and release parameters at the frog sensory-motor synapse. J Physiol London 1984;349:459–74.

Harmon HH. Modern factor analysis. 3rd ed. Chicago: University of Chicago Press; 1979.

Harris KM, Kater SB. Dendritic spines—cellular specializations imparting both stability and flexibility to synaptic function. Ann Rev Neurosci 1994;17:341–71.

Henery RJ, Robinson J, Bennett MR. Methods for grouping shapes of synaptic currents recorded from sets of synapses. J Neurosci Methods 1998;86:79–90.

Hessler NA, Shirke AM, Malinow R. The probability of transmitter release at a mammalian central synapse. Nature 1993;366:569–72.

Horn R, Marty A. Muscarinic activation of ionic currents measured by a new whole-cell recording method. J Gen Physiol 1988;92:145–59.

Hotelling H. Analysis of a complex of statistical variables into principal components. J Educ Psychol 1933;24:417–41 and 498–520.

Huang EP, Stevens CF. Estimating the distribution of synaptic reliabilities. J Neurophysiol 1997;78:2870–80.

Isaac JTR, Nicoll RA, Malenka RC. Evidence for silent synapses: implications for the expression of LTP. Neuron 1995;16:427–34.

Jack JJ, Larkman AU, Major G, Stratford KJ. Quantal analysis of the synaptic excitation of CA1 hippocampal pyramidal cells. Adv Second Messenger Phosphoprotein Res 1994;29:275–99.

Jackson JE. A user's guide to principal components. New York: Wiley; 1991.

Kasyanov AM, Maximov VV, Byzov AL, Berretta N, Sokolov MV, Gasparini S, Cherubini E, Reymann K, Voronin LL. Intrasynaptic ephaptic feedback alters amplitude-voltage relations of mossy fibre responses in rat CA3 hippocampal neurones. Neuroscience 2000;101:323–36.

Kleschevnikov AM, Sokolov MV, Kuhnt U, Dawe GS, Stephenson JD, Voronin LL. Changes in paired-pulse facilitation correlated with induction of long-term potentiation in area CA1 of rat hippocampal slices. Neuroscience 1997;76:829–43.

Kleschevnikov AM, Kuhnt U, Voronin LL. Quantal analysis of a late phase of long-term potentiation in the guinea pig hippocampal slices. Neurosci Res Commun 2002;30:7–25.

Korn H, Faber DS. Regulation and significance of probabilistic release mechanisms at central synapses. In: Edelman H, editor. Synaptic function. New York: Wiley; 1987.

Korn H, Faber DS. Quantal analysis and synaptic efficacy in the CNS. Trends Neurosci 1991;14:439–45.

Kuhnt U, Voronin LL. Interaction between paired-pulse facilitation and long-term potentiation in area CA1 of guinea pig hippocampal slices: application of quantal analysis. Neuroscience 1994;62:391–7.

Kullmann DM. Quantal variability of excitatory transmission in the hippocampus: implications for the opening probability of fast glutamate-gated channels. Proc R Soc London B: Biol Sci 1993;253:107–16.

Kullmann DM, Erdemli G, Asztely F. LTP of AMPA and NMDA receptor-mediated signals: evidence for presynaptic expression and extrasynaptic glutamate spill-over. Neuron 1996;17:461–74.

Larkman A, Hannay T, Stratford K, Jack J. Presynaptic release probability influences the locus of long-term potentiation. Nature 1992;360:70–3.

Li S, Anwyl R, Rowan MJ. A persistent reduction in short-term facilitation accompanies long-term potentiation in the CA1 area in the intact hippocampus. Neuroscience 2000;100:213–20.

Liao D, Jones A, Malinow R. Direct measurement of quantal changes underlying long-term potentiation in CA1 hippocampus. Neuron 1992;9:1089–97.

Liu G, Tsien RW. Properties of synaptic transmission at single hippocampal synaptic boutons. Nature 1995;375:404–8.

Luscher C, Frerking M. Restless AMPA receptors: implications for synaptic transmission and plasticity. Trends Neurosci 2001;24:665–70.

Magee JC, Johnston D. Synaptic activation of voltage-gated channels in the dendrites of hippocampal pyramidal neurons. Science 1995;268:301–4.

Magleby KL, Miller DC. Is the quantum of transmitter release composed of subunits? A critical analysis in the mouse and frog. J Physiol London 1981;311:267–87.

Malenka RC, Nicoll RA. Long-term potentiation. A decade of progress? Science 1999;285:1870–4.

Malinow R. Transmission between pairs of hippocampal slice neurons: quantal levels, oscillations, and LTP. Science 1991;252:722–4.

Markram H, Lubke J, Frotscher M, Roth A, Sakmann B. Physiology and anatomy of synaptic connections between thick tufted pyramidal neurones in the developing rat neocortex. J Physiol London 1997;500:409–40.

Musial P, Kublik E, Wrobel A. Spontaneous variability reveals principal components in cortical evoked potentials. NeuroReport 1998;9:2627–31.

Neher E, Sakaba T. Estimating transmitter release rates from postsynaptic current fluctuations. J Neurosci 2001;21:9638–54.

Neher E, Sakaba T. Combining deconvolution and fluctuation analysis to determine quantal parameters and release rates. J Neurosci Methods 2003;130:143–57.

Nicholls JG, Martin AR, Wallace BG, Fuchs PA. From neuron to brain. Sunderland, MA: Snauer; 2001.

Press WH, Flannery BP, Teukolsky SA, Vetterling WT. Numerical recipes. Cambridge: Cambridge University Press; 1986.

Raastad M. Extracellular activation of unitary excitatory synapses between hippocampal CA3 and CA1 pyramidal cells. Eur J Neurosci 1995;7:1882–8.

Redman S. Quantal analysis of synaptic potentials in neurons of the central nervous system. Physiol Rev 1990;70:165–98.

Rosenmund C, Clements JD, Westbrook GL. Nonuniform probability of glutamate release at a hippocampal synapse. Science 1993;262:754–7.

Rusakov DA. Quantal behaviour of synaptic transmission can be statistically examined using the Fourier line spectrum of the histogram of synaptic potentials. Neurosci Lett 1993;163:231–4.

Saviane C, Savtchenko LP, Raffaelli G, Voronin LL, Cherubini E. Frequency-dependent modulation of paired-pulse ratio at unitary CA3–CA3 synapses in the rat hippocampus. J Physiol London 2002;544:469–76.

Sayer RJ, Friedlander MJ, Redman SJ. The time course and amplitude pairs of EPSPs evoked at synapses between pairs of CA3/CAI neurons in the hippocampal slice. J Neurosci 1990;10:826–36.

Schneggenburger R, Sakaba T, Neher E. Vesicle pools and short-term synaptic depression: lessons from a large synapse. Trends Neurosci 2002;25:206–12.

Schulz PE. Long-term potentiation involves increases in the probability of neurotransmitter release. Proc Natl Acad Sci USA 1997;94:5888–93.

Sokolov MV, Rossokhin AV, Behnisch T, Reymann KG, Voronin LL. Interaction between paired-pulse facilitation and long-term potentiation of minimal EPSPs in rat hippocampal slices: a patch clamp study. Neuroscience 1998;85:1–13.

Sokolov MV, Rossokhin AV, Astrelin AV, Frey JU, Voronin LL. Quantal analysis suggests a strong involvement of presynaptic mechanisms during the initial 3 h maintenance of long-term potentiation in rat hippocampal CA1 area in vitro. Brain Res 2002;957:61–75.

Sokolov MV, Rossokhin AV, Kasyanov AM, Gasparini S, Berretta N, Cherubini E, Voronin LL. Associative mossy fibre LTP induced by pairing presynaptic stimulation with postsynaptic hyperpolarization of CA3 neurones in rat hippocampal slice. Eur J Neurosci 2003;17:1425–37.

Stern P, Edwards FA, Sakmann B. Fast and slow components of unitary EPSCs on cells elicited by focal stimulation in slices of cortex. J Physiol London 1992;449:247–78.

Stevens CF. Quantal release of neurotransmitter and long-term potentiation. Cell/Neuron 1993;70(Suppl):55–63.

Stratford KJ, Tarczy-Hornoch K, Martin KA, Bannister NJ, Jack JJB. Excitatory synaptic inputs to spiny stellate cells in cat visual cortex. Nature 1996;382:258–62.

Stratford KJ, Jack JJ, Larkman AU. Calibration of an autocorrelation-based method for determining amplitude histogram reliability and quantal size. J Physiol London 1997;505:425–42.

Stricker C, Redman SJ. Quantal analysis based on density estimation. J Neurosci Methods 2003;103:159–71.

Stricker C, Redman S, Daley D. Statistical analysis of synaptic transmission: model discrimination and confidence limits. Biophys J 1994;67:532–47.

Stricker C, Field AC, Redman SJ. Statistical analysis of amplitude fluctuations in EPSCs evoked in rat CA1 pyramidal neurones in vitro. J Physiol London 1996a;490:419–41.

Stricker C, Field AC, Redman S. Changes in quantal parameters of EPSCs in rat CA1 neurones in vitro after the induction of long-term potentiation. J Physiol London 1996b;490:443–54.

Stuart GJ, Dodt H-U, Sakmann B. Patch-clamp recordings from the soma and dendrites of neurons in brain slices using infrared video microscopy. Pflugers Arch 1993;423:511–8.

Thomson AM. Molecular filters at central synapses. Prog Neurobiol 2000;62:159–96.

Thomson AM, Deuchars J. Diverse pre- and post-synaptic properties of fast excitatory synapses. In: Thomson AM, Deuchars J, editors. Excitatory amino acids and synaptic transmission. London: Academic Press; 1995. p. 146–72.

Torii N, Tsumoto T, Uno L, Astrelin AV, Voronin LL. Quantal analysis suggests presynaptic involvement in expression of neocortical short- and long-term depression. Neuroscience 1997;79:317–21.

Volgushev M, Voronin LL, Chistiakova M, Artola A, Singer W. All-or-none excitatory postsynaptic potentials in the rat visual cortex. Eur J Neurosci 1995;7:1751–60.

von Gersdorff H, Borst JG. Short-term plasticity at the calyx of held. Nat Rev Neurosci 2002;3:53–64.

Voronin LL. Long-term potentiation in the hippocampus. Neuroscience 1983;10:1051–69.

Voronin LL. On the quantal analysis of hippocampal long-term potentiation and related phenomena of synaptic plasticity. Neuroscience 1993a;56:275–304.

Voronin LL. Synaptic modifications and memory. An electrophysiological analysis. Berlin: Springer; 1993b. p. 1–303.

Voronin LL. Quantal analysis of hippocampal long-term potentiation. Rev Neurosci 1994;5:141–70.

Voronin LL, Cherubini E. Presynaptic silence may be golden. Neuropharmacology 2003;45:1–10.

Voronin LL, Kuhnt U, Hess G, Gusev AG, Roschin V. Quantal parameters of “minimal” excitatory postsynaptic potentials in guinea pig hippocampal slices: binomial approach. Exp Brain Res 1992a;89:248–64.

Voronin LL, Kuhnt U, Gusev AG. Analysis of fluctuations of “minimal” excitatory postsynaptic potentials during long-term potentiation in guinea pig hippocampal slices. Exp Brain Res 1992b;89:288–99.

Voronin L, Byzov A, Kleschevnikov A, Kozhemyakin M, Kuhnt U, Volgushev M. Neurophysiological analysis of long-term potentiation in mammalian brain. Behav Brain Res 1995;66:45–52.

Voronin LL, Volgushev M, Chistiakova M, Kuhnt U, Singer W. Involvement of silent synapses in the induction of LTP and LTD in hippocampal and neocortical neurones. Neuroscience 1996;74:323–30.

Voronin LL, Volgushev M, Sokolov M, Kasyanov A, Chistiakova M, Reymann KG. Evidence for an ephaptic feedback in cortical synapses: postsynaptic hyperpolarization alters the number of response failures and quantal content. Neuroscience 1999;92:399–405.

Walmsley B. Quantal analysis of synaptic transmission. In: Wallis DI, editor. Electrophysiology—a practical approach. Oxford: IRL Press; 1993. p. 110–41.

Walmsley B, Edwards FR, Tracey DJ. Nonuniform release probabilities underlie quantal synaptic transmission at a mammalian excitatory central synapse. J Neurophysiol 1988;60:889–908.

Zefirov AL, Stolov EL. Model of mediator secretion at a neuromuscular synapse based on the spatial heterogeneity of the probability of acetylcholine quantum release. Neurophysiology/Neirofiziologiia 1982;14:233–40.